Redox Biology 56 (2022) 102447

Contents lists available at ScienceDirect

Redox Biology

journal homepage: www.elsevier.com/locate/redox

The coupling of mitoproteolysis and oxidative phosphorylation enables tracking of an active mitochondrial state through MitoTimerfluorescence

Yinyin Xie [1], Yannan Zhang [1], Aina Sun [1], Yamei Peng, Weikang Hou, Cong Xiang, Guoxin Zhang [2], Beibei Lai, Xiaoshuang Hou, Fangfang Zheng, Fan Wang, Geng Liu [*]

State Key Laboratory of Pharmaceutical Biotechnology, MOE Key Laboratory of Model Animals for Disease Study and Jiangsu Key Laboratory of Molecular Medicine, Model Animal Research Center, School of Medicine, Nanjing University, 12 Xuefu Road, Pukou High-Tec District, Nanjing, JiangSu Province, 210061, China

ARTICLE INFO

Keywords:
Mitoproteolysis
MitoTimer
Oxidative metabolism
PGC-1α
Muscle fiber type

ABSTRACT

The regulation of mitochondria function and health is a central node in tissue maintenance, ageing as well as the pathogenesis of various diseases. However, the maintenance of an active mitochondrial functional state and its quality control mechanisms remain incompletely understood. By studying mice with a mitochondria-targeted reporter that shifts its fluorescence from "green" to "red" with time (MitoTimer), we found MitoTimer fluorescence spectrum was heavily dependent on the oxidative metabolic state in the skeletal muscle fibers. The mitoproteolytic activity was enhanced in an energy dependent manner, and accelerated the turnover of MitoTimer protein and respiratory chain substrate, responsible for a green predominant MitoTimer fluorescence spectrum under the oxidative conditions. PGC1α, as well as anti-ageing regents promoted enhanced mitoproteolysis. In addition, cells with the green predominant mitochondria exhibited lower levels of MitoSox and protein carbonylation, indicating a favorable redox state. Thus, we identified MitoTimer as a probe for mitoproteolytic activity *in vivo* and found a heightened control of mitoproteolysis in the oxidative metabolic state, providing a framework for understanding the maintenance of active oxidative metabolism while limiting oxidative damages.

1. Introduction

Mitochondria are important organelles for supply of cellular energy through respiration and regulation of cellular metabolism and redox state [1,2]. The dysfunction of mitochondria, while promoting oxidative stresses, has been reported in many human diseases, including cardiac dysfunction, metabolic and neurodegenerative diseases [3–5]. To maintain their health, mitochondria engage in several dynamic behaviors for quality control [6,7]. Mitoproteostasis, regarded as the first line of defense against a mild mitochondrial damage, involves the processing and correct folding of imported proteins and the degradation of the misfolded or oxidized proteins [8]. Pathogenic mutations in mitoprotease encoding genes are associated with a plethora of neurodegenerative disorders [9]. The transcriptional regulation of the executing genes in mitoproteostasis under stress conditions, referred as the mitoUPR, has attracted much attention. Although mitoUPR was first addressed by forced expression of ΔOTC protein aggregates in the mitochondrial matrix of mammalian cells [10], it is extensively and delicately studied in the *C. elegans*, found to be essential for life span extension and longevity, and controlled by ATFS-1, which altered its localization from mitochondria to nucleus upon stress [11]. In contrast, a few chaperons and mitoproteases were mildly induced in mammals under certain mitochondrial stress conditions, possibly linked to the Integrated Stress Response (ISR) [12,13]. Interestingly, increased NAD^+ levels, associated with a mitochondria-nuclear encoded protein imbalance, clearly promoted mitoUPR and resulted in significant health benefits in mammals [14–16]. However, beyond the regulation at the transcriptional level, it is difficult to determine the mitoproteolytic activity *in situ* in various *in vivo* contexts, thus hindering the probing of the intrinsic regulation of mitoproteostasis at physiological level.

Skeletal muscle, known for its importance in energy expenditure and metabolic regulation, is one of the most dynamic and plastic tissues in

* Corresponding author.
E-mail address: liug53@nju.edu.cn (G. Liu).
[1] These authors contributed equally to this work.
[2] Current address: Division of Regenerative Medicine, Department of Medicine, Moores Cancer Center and Sanford Consortium for Regenerative Medicine, University of California, San Diego, California.

https://doi.org/10.1016/j.redox.2022.102447
Received 3 May 2022; Received in revised form 29 July 2022; Accepted 12 August 2022
Available online 18 August 2022

the body. Its heterogeneity was illustrated by the significant variability in the biochemical, mechanical, and metabolic state of individual fibers. Slow-twitch oxidative fibers exhibit high mitochondrial content, increased reliance on oxidative phosphorylation (OXPHOS), and high resistance to fatigue. In contrast, fast-twitch glycolytic fibers exhibit lower mitochondrial content, decreased reliance on oxidative phosphorylation, and low resistance to fatigue [17]. In addition, mitochondrial dynamics including fission and fusion is tightly linked to the cellular metabolic state, with oxidative fibers having more elongated and connected mitochondria than the glycolytic fibers [18]. The regulation of mitochondrial quality control mechanisms in metabolically distinctive muscle fibers remains obscure and skeletal muscle may provide an excellent model to study the regulation of mitoproteostasis and mitophagy for mitochondrial quality control under distinct physiological metabolic contexts.

MitoTimer is a DsRed variant targeted to the mitochondrial matrix that changes its fluorescence spectrum from green to red with time due to the oxidation (dehydrogenization) of its Tyr-67 residue [19,20]. As such, the green fluorescence of MitoTimer represents the relatively "young" protein while its red fluorescence represents the "old" protein, and the green/red fluorescence ratio as reflected in MitoTimer fluorescence spectrum was expected to reveal time-associated aspects of mitochondria [21]. In principle, changes in the cellular redox state may affect the green-to-red transition of MitoTimer fluorescence. However, existing reports suggested that only dramatic changes in PH or oxygen tension were able to affect this transition [21–23]. Therefore, how the equilibrium of the red/green MitoTimer fluorescence is determined and maintained under homeostatic conditions remain elusive, given the observations of *in vivo* heterogeneity and alteration of the MitoTimer fluorescence spectrum [23,24]. A recent report indicated a close link between a green predominant MitoTimer fluorescence spectrum with reduced oxidative stress and suggested MitoTimer fluorescence might indicate mitochondrial health [22]. Thus, an important task would be to identify the major determining factor(s) influencing MitoTimer fluorescence spectrum under physiological conditions and further reveal the specific functional aspects of mitochondrial state as measured by MitoTimer fluorescence *in vivo*.

In this study, we established BAC transgenic mice expressing MitoTimer to study the dynamic aspects of mitochondria in the skeletal muscle *in vivo*. We found a remarkable green predominant MitoTimer fluorescent spectrum in the oxidative muscle and fiber types compared to their glycolytic counterparts. Tissue culture experiments further confirmed the strong metabolic influence on MitoTimer fluorescence spectrum. Critically, we found the mitoproteolytic activity was elevated under active oxidative metabolic conditions, resulting in accelerated turnover of MitoTimer protein and a green predominant MitoTimer fluorescence. Mechanistically, the Sirtuin/PGC-1α pathway coordinately regulated mitoproteolytic activity and mitochondrial oxidative metabolism. The intrinsically coupled mechanisms as marked by the green predominant MitoTimer fluorescence provided new insight for the role of mitoproteostasis in the quality control of highly active mitochondria.

2. Results

2.1. The heterogeneity of MitoTimer fluorescence spectrum was directly linked to metabolically distinctive skeletal muscle fiber types

To examine the nature and determinant of MitoTimer fluorescence spectrum in mouse skeletal muscles, we generated MitoTimer BAC transgenic mice in which an expression cassette containing a MitoTimer reporter together with both a tetracycline/doxycycline inducible system and loxP-STOP-loxP elements was inserted between exon1 and exon2 of a BAC ROSA26 gene locus, followed by pronucleus microinjection of the BAC construct in the mouse zygotes (Fig. S1A). EIIa-cre mice were crossed with MitoTimer BAC transgenic mice to generate mice with the deletion of the "STOP" cassette for expression of MitoTimer in multiple tissues under the control of doxycycline (referred to as dMT mice) (Fig. S1A). Mouse embryonic fibroblast (MEF) cells derived from the dMT mice were exposed to doxycycline to induce MitoTimer expression for 24 h, and were cultured without doxycycline for additional 24 and 48 h. As predicted, the MitoTimer fluorescence spectrum of the MEFs shifted from green to red with time (Fig. S1B). Flow cytometry analysis confirmed the fluorescence spectrum shift (Fig. S1C). To examine whether MitoTimer expression perturbed mitochondrial function, we measured oxygen consumption rate and found no difference between wild-type (WT) and dMT MEFs under doxycycline treatment (Fig. S1D).

We studied MitoTimer fluorescence spectrum in skeletal muscles of the dMT mice fed with 0.2% doxycycline in drinking water from one month of age and lasted for 2 months. While the fluorescence images were acquired with identical parameters for all samples from the same mouse, MitoTimer fluorescence spectrum exhibited apparent heterogeneity among different type of skeletal muscles. We found a highly consistent green predominant MitoTimer fluorescence spectrum (lower red-to-green ratio) in soleus muscles compared with that of *extensor digitorum longus* (EDL) muscles in cross-sections (Fig. 1A). Upon examination of the muscle vertical-sections, the slow-twitch and oxidative soleus and diaphragm (DIA) muscles with typically elongated and interconnected mitochondria also exhibited a distinct green predominant fluorescence spectrum compared with the EDL and the *tibialis anterior* (TA) muscles, which were fast-twitch glycolytic skeletal muscles with mostly small block-like mitochondria (Fig. 1B). Furthermore, the green predominant MitoTimer fluorescence spectrum in the soleus fibers were also observed in freshly prepared muscles and their sections (Figs. S2A-D, E-J). We also noted that within the same muscles, two neighboring muscle fibers, if with distinctive mitochondrial morphology, also exhibited a differential fluorescence spectrum (Fig. 1C). The muscle fiber with elongated mitochondria exhibited a green predominant fluorescence spectrum compared with the muscle fiber showing fragmented mitochondria (Fig. 1B). As skeletal muscle is composed of mixed fiber types, the above observations raised the possibility that the MitoTimer fluorescence heterogeneity may be linked to muscle fiber types.

We directly examine the MitoTimer fluorescence spectrum of muscle fibers in different types of muscles using cross-sections. Again, the overall red-to-green ratio of MitoTimer fluorescence was higher in EDL compared with that in soleus (Fig. 1D and E). In addition, both EDL and soleus muscles displayed a high degree of inter-heterogeneity for individual fibers in MitoTimer fluorescence spectrum (Fig. 1D). By recording the fluorescence of individual fibers in the cross-sections, the MitoTimer fluorescence spectrum of the EDL fibers displayed a significantly higher red-to-green ratio compared with that of the soleus fibers (Fig. 1F). A heat map to recapitulate the fluorescence red-to-green ratio of EDL and soleus fibers in the cross sections also showed a skewed distribution of fluorescence spectrum between the two types of muscles (Fig. 1G). Type1, type 2A, type 2X and type 2B are the four major fiber types in rodent skeletal muscles identified by their distinct distribution of myosin heavy chain (MyHC) composition and exhibit sequentially decreased oxidative capacity. The mouse EDL muscle consists of predominantly glycolytic type 2B and 2X fibers and a small population of oxidative 2A fibers whereas soleus muscle is composed essentially of oxidative type 1 and 2A fibers. MyHC immunofluorescence staining was performed to identify Type 1, 2A and 2B fiber types in the dMT muscle cross-sections. In soleus muscle, the most oxidative type 1 fibers exhibited a lower red-to-green fluorescence ratio than type 2A fibers (Fig. 1H and I). In EDL muscles, type 2B fibers, which are more glycolytic, exhibited a higher red-to-green fluorescence ratio than type 2A fibers (Fig. 1H and I). The red-to-green fluorescence ratios of type 2A were comparable in both soleus and EDL muscles (Fig. 1I). Quantitatively, the three skeletal muscle fibers formed a continuum in terms of red-to-green fluorescence ratio, with type 1< type 2A < type 2B, paralleling their oxidative capacity (Fig. 1I and J). Thus, the heterogeneity in MitoTimer fluorescence

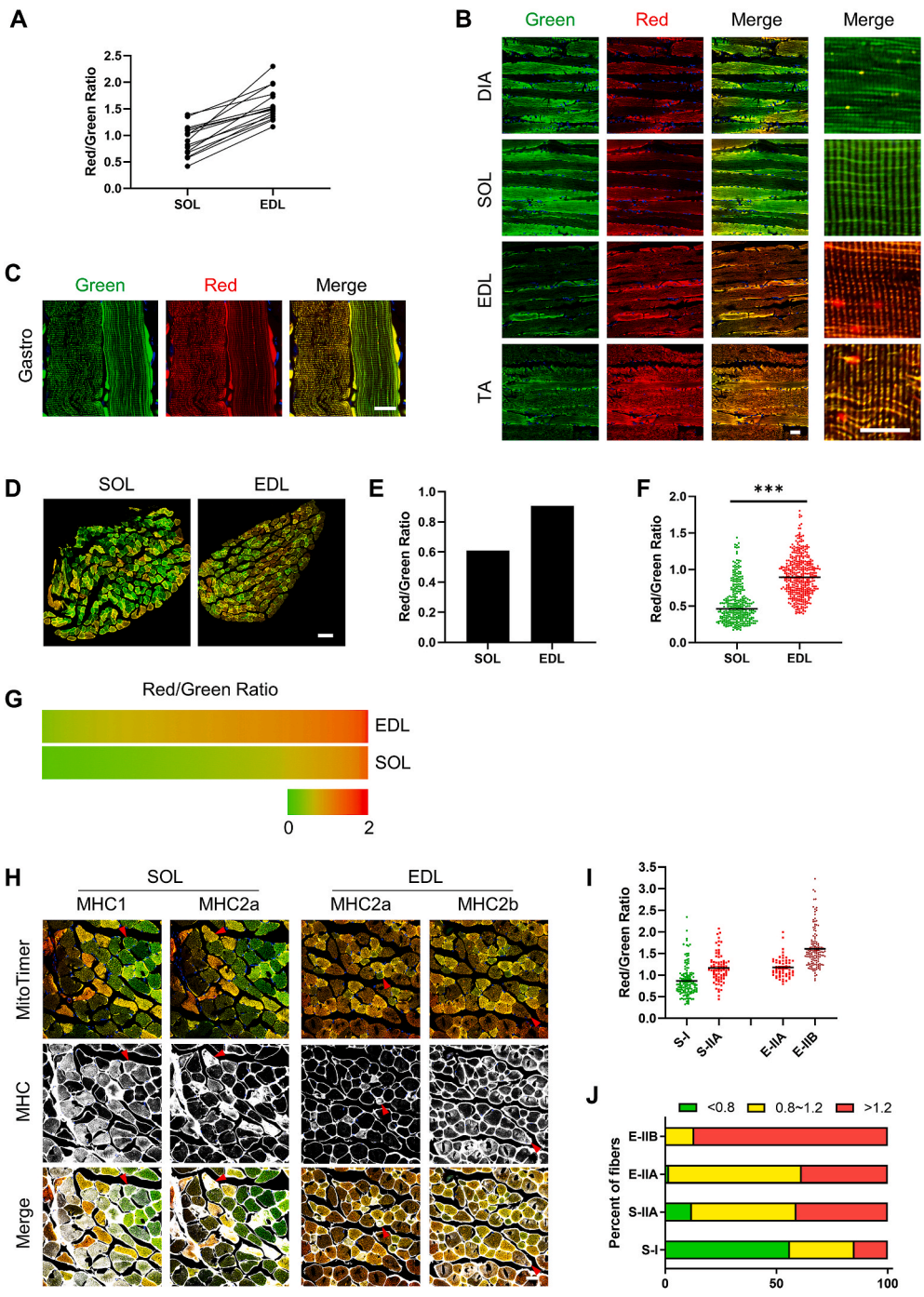

Fig. 1. The heterogeneity of MitoTimer fluorescence spectrum was directly linked to metabolically distinctive skeletal muscle fiber types. (A) The ratio of MitoTimer red/green fluorescence intensities in the cross-section of soleus and EDL muscles from dMT mice (n = 15). Soleus and EDL muscles isolated from individual mouse were photographed with identical predetermined acquisition parameters at one time. (B) Representative MitoTimer fluorescence images in the vertical-sections of muscles from individual mouse following doxycycline induction from 1 month to 3 months of age (n = 6). Scale bar, 50 μm in the left panels and 20 μm in the right panels. (C) Heterogeneity of MitoTimer fluorescence spectrum in the two neighboring fibers from gastrocnemius (Gastro) muscle. Scale bar, 30 μm. (D) Images of MitoTimer fluorescence in cross-section of muscle fibers from soleus and EDL muscles. Scale bar, 200 μm (E) Quantification of the ratio of the red/green fluorescence intensities in (D). (F) Quantification of the ratio of the red/green fluorescence intensities in single fibers from the soleus and EDL muscles in (D). (G) Schematic representations of the ratio of the red/green fluorescence intensities in single muscle fiber in (F).(H) RepresentativeMHC1, MHC2A and MHC2B immunofluorescence staining images of soleus and EDL muscles showing type 1, type 2A and type 2B muscle fibers with distinct MitoTimer fluorescence spectrum (n = 5). Arrows indicate fibers positive for the specific fiber type marker. Scale bar, 50 μm(I) Quantifications of the ratio of the red/green fluorescence intensities in MHC1, MHC2A and MHC 2B fibers of soleus and EDL muscles, respectively. (J) Distribution of green, intermediate and red predominance of MitoTimer fluorescence spectrum according to the values in (I) in MHC1, MHC2A and MHC 2B fibers of soleus and EDL muscles, respectively. Data are presented as mean ± SEM. *p < 0.05, **p < 0.01, ***p < 0.001 (*t*-test). (For interpretation of the references to colour in this figure legend, the reader is referred to the Web version of this article.)

spectrum found in the soleus and EDL muscles can be attributed to the distinct fluorescence spectrum in their composite fiber types. These results revealed a clear distinction of MitoTimer fluorescent spectrum in the metabolically distinct fibers, suggesting a possible link between the metabolic states and MitoTimer fluorescence spectrum.

2.2. *MitoTimer fluorescence spectrum was strongly influenced by the oxidative energetic state in vivo and in vitro*

The fiber type profile of skeletal muscles undergoes significant changes in mouse postnatal life. Neonatal myofibers contain a significant proportion of slow type fibers and exhibit uniformly high oxidative activity [17,25]. Therefore, we wondered whether MitoTimer fluorescence spectrum also respond to their distinct oxidative capacities during developmental stages. Indeed, postnatal day 14 mice showed a predominant green fluorescence spectrum in TA skeletal muscles compared with those from the 12-week-old mice (Fig. 2A and B). Endurance exercise is reported to induce increased respiratory capacity and fiber-type switching in certain hindlimb muscles including the plantaris muscle [18,26]. After 4 weeks of voluntary running, the MitoTimer fluorescence spectrum in the plantaris muscle of the dMT mice shifted to a lower red-to-green ratio compared with the control group (Fig. 2C and D), consistent with the finding of MitoTimer fluorescence shift after exercise in the mouse flexor digitorum brevis (FDB) muscle [22]. These results suggested that the MitoTimer fluorescence spectrum closely paralleled the change of cellular oxidative capacity in muscle fibers *in vivo*.

C2C12 myoblasts are commonly used as an *in vitro* system to study muscle differentiation and metabolism. We generated C2C12 cell lines

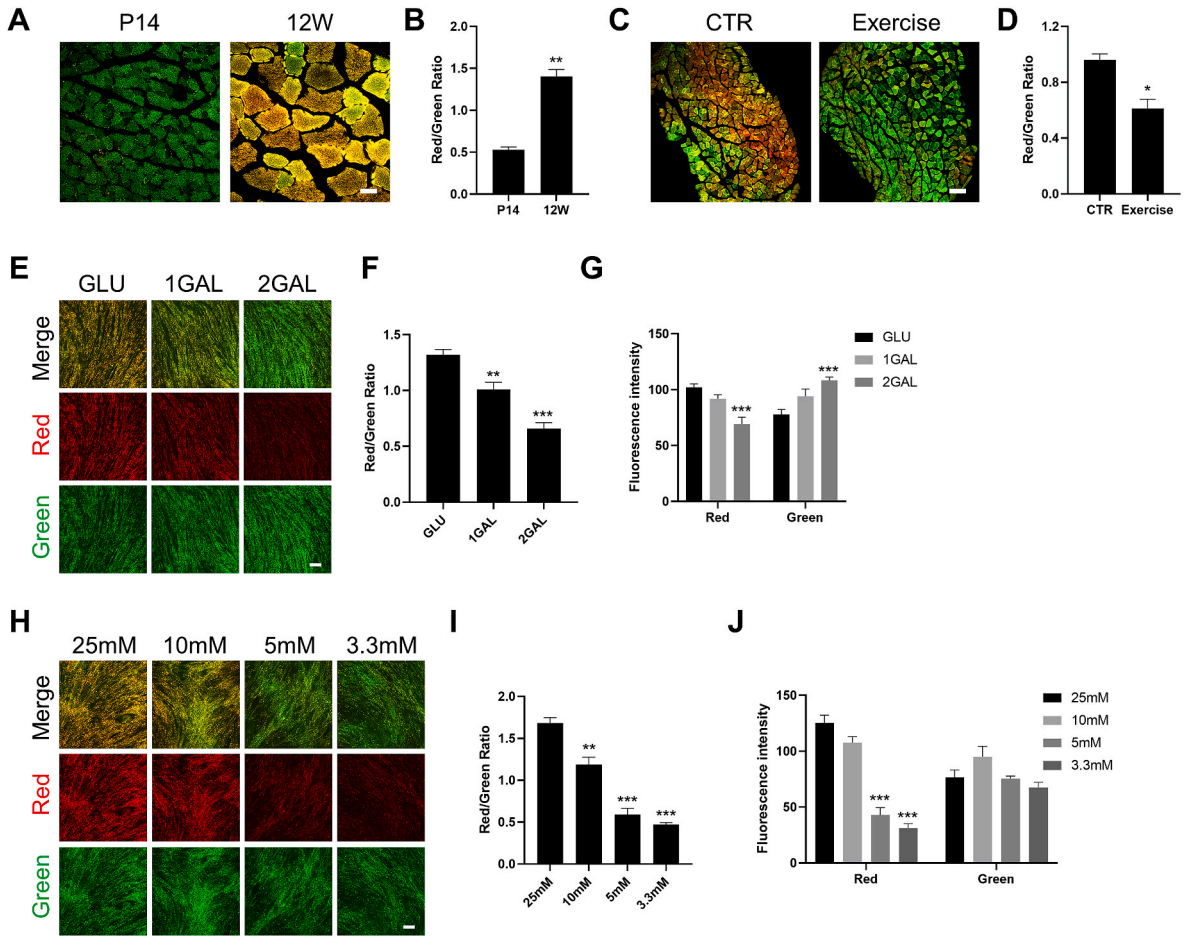

Fig. 2. MitoTimer fluorescence spectrum was strongly influenced by the oxidative metabolic state *in vivo* and *in vitro*. (A) MitoTimer fluorescence spectrum of TA muscles from P14 and 12-week-old mice. Scale bar, 50 μm. (B) Quantification of the ratio of the red/green fluorescence intensities in TA muscles from P14 and 12-week-old mice (n = 3). (C) MitoTimer fluorescence spectrum of the plantaris muscles from sedentary and exercised mice. Scale bar, 200 μm. (D) Quantification of the ratio of the red/green fluorescence intensities in the plantaris muscles from sedentary and exercised mice (n = 3). (E) Representative MitoTimer fluorescence images of MitoTimer-C2C12 myotubes cultured in GLU and GAL-rich medium. 1GAL and 2GAL denoted the mixing ratio of GLU and GAL in the medium. Scale bar, 200 μm. (F) Quantification of the ratio of the red/green fluorescence intensities in MitoTimer-C2C12 myotubes cultured in GLU and GAL-rich medium . (G) Quantification of green and red fluorescence intensities in MitoTimer-C2C12 myotubes cultured in GLU and GAL-rich medium (n = 3). (H) Representative MitoTimer fluorescence images of MitoTimer-C2C12 myotubes cultured in glucose-gradient media. Scale bar, 200 μm. (I) Quantification of the ratio of the red/green fluorescence intensities in MitoTimer-C2C12 myotubes cultured in glucose-gradient media . (J) Quantification of green and red fluorescence intensities in MitoTimer-C2C12 myotubes cultured in glucose-gradient media (. Data are presented as mean ± SEM. *p < 0.05, **p < 0.01, ***p < 0.001 (*t*-test). (For interpretation of the references to colour in this figure legend, the reader is referred to the Web version of this article.)

expressing MitoTimer upon doxycycline induction. To investigate the link between MitoTimer fluorescence spectrum and cellular metabolic states, we analyzed MitoTimer fluorescence spectrum in C2C12 cells under culture conditions to induce either high or low OXPHOS activities. Galactose (GAL) or Acetoacetate (ACE) media substantially switched cells to a more oxidative metabolic state [27,28]. We found the media containing 3.3 mM Galactose/6.7 mM Glucose and 6.7 mM Galactose/3.3 mM Glucose (referred to as 1 GAL and 2GAL, respectively) supported the long-term culture of C2C12 cells and the 2GAL medium significantly increased the oxygen consumption of the MitoTimer-C2C12 cells compared to the medium containing 10 mM Glucose (GLU) (Fig. S3A). The differentiated MitoTimer-C2C12 myotubes were cultured for 4 days in the GLU, 1GAL, 2GAL media with the treatment of doxycycline to induce MitoTimer expression for the last 2 days. With the increased levels of Galactose in the culture medium, the cells exhibited sequentially decreased red-to-green ratios of MitoTimer fluorescence (Fig. 2E and F). Quantification of the fluorescence intensity revealed that the red fluorescence was significantly decreased with the green fluorescence increased in the 2GAL medium (Fig. 2G). MitoTimer-C2C12 myotubes exhibited similar difference in the fluorescence spectrum when cultured in the ACE-rich medium compared to that in the GLU medium (Figs. S3B–D). Notably, FACS on the isolated mitochondria from both the cells cultured in the 2GAL medium and soleus muscle validated the green predominant MitoTimer spectrum found in the cells and the tissue and suggested that MitoTimer fluorescence spectrum was independent of mitochondrial quantity (Fig. S3E). As low glucose concentration in culture medium represents a nutrient stress condition and enhanced mitochondrial oxidative metabolism of cells (Fig. S3F) [28,29], we cultured MitoTimer-C2C12 myotubes with 25 mM, 10 mM, 5 mM and 3.3 mM glucose in medium respectively, and found a sequential shift to the green-predominant MitoTimer fluorescent spectrum (Fig. 2H and I). Notably, the red fluorescence was also sequentially decreased whereas the green fluorescence did not significantly change (Fig. 2J). Furthermore, although the mRNA expression levels of MitoTimer in the MitoTimer-C2C12 myotubes varied under different culture conditions and doxycycline treatment schemes (Figs. S3G and S3I), different expression levels of MitoTimer resulting from the alterations of either the dose or length of doxycycline treatments did not appear to affect the green-predominant MitoTimer fluorescence spectrum in cells cultured in the oxidative medium as

compared to that in the high glucose medium (Figs. S3H, S3J-K). Therefore, the oxidative metabolic state and its alteration strongly influence MitoTimer fluorescence spectrum both *in vivo* and *in vitro*. Cells in a more oxidative metabolic state were directly associated with a green-predominant MitoTimer fluorescence spectrum.

2.3. The green predominant fluorescence spectrum of MitoTimer was not directly linked to selective mitophagy in the skeletal muscle fibers in vivo

Mitophagy, which is supposed to eliminate damaged mitochondria, was suggested to play an important role in cultured cells with high OXPHOS activity [30]. However, it is not clear whether skeletal muscle fibers with distinct metabolic profiles correlated with different mitophagic flux. The red puncta found in the MitoTimer expressing muscle fibers were suggested to represent depolarized mitochondria in mitophagosomes [22]. We also found that muscle fibers in the dMT mice contained puncta marked with strong red or yellow fluorescence (Fig. 3A) and stained positive for both LC3B and LAMP-1 (Fig. 3D and E), indicating that these puncta represented the mitochondria undergoing mitophagy in the autolysosome. Interestingly, the number of red puncta was significantly less in soleus muscles compared with that in EDL muscles (Fig. 3B). Further, there was significantly fewer number of red puncta in type 1 fibers compared with the type 2A fibers within soleus muscle, and the number of puncta in the type 2A fibers was fewer compared to that of type 2B fibers within EDL muscle (Fig. 3C). Chloroquine (CQ), used for measuring autophagic flux by its ability to block the autophagic degradation pathway [31], was administered intraperitoneally in dMT mice for 3 consecutive days. While Chloroquine treatment led to the increased levels of LC3B and p62 proteins (Fig. S3L), together with a dramatic accumulation of red puncta in both soleus and EDL muscles (Fig. 3F), soleus muscle still contained significantly fewer red puncta than the EDL muscle (Fig. 3G). Intriguingly, the fact that the most oxidative type 1 fibers exhibited the least mitophagy and red puncta may otherwise suggest that mitochondria in the oxidative fibers were protected with other quality control mechanisms. It raised the possibility that an enhanced first line quality control mechanism by mitoproteostasis was actively operating in this type of fibers.

2.4. Enhanced mitoproteolytic activities in cells and muscles with high OXPHOS activity

Naturally, when proteins are accessible to the proteolytic machinery

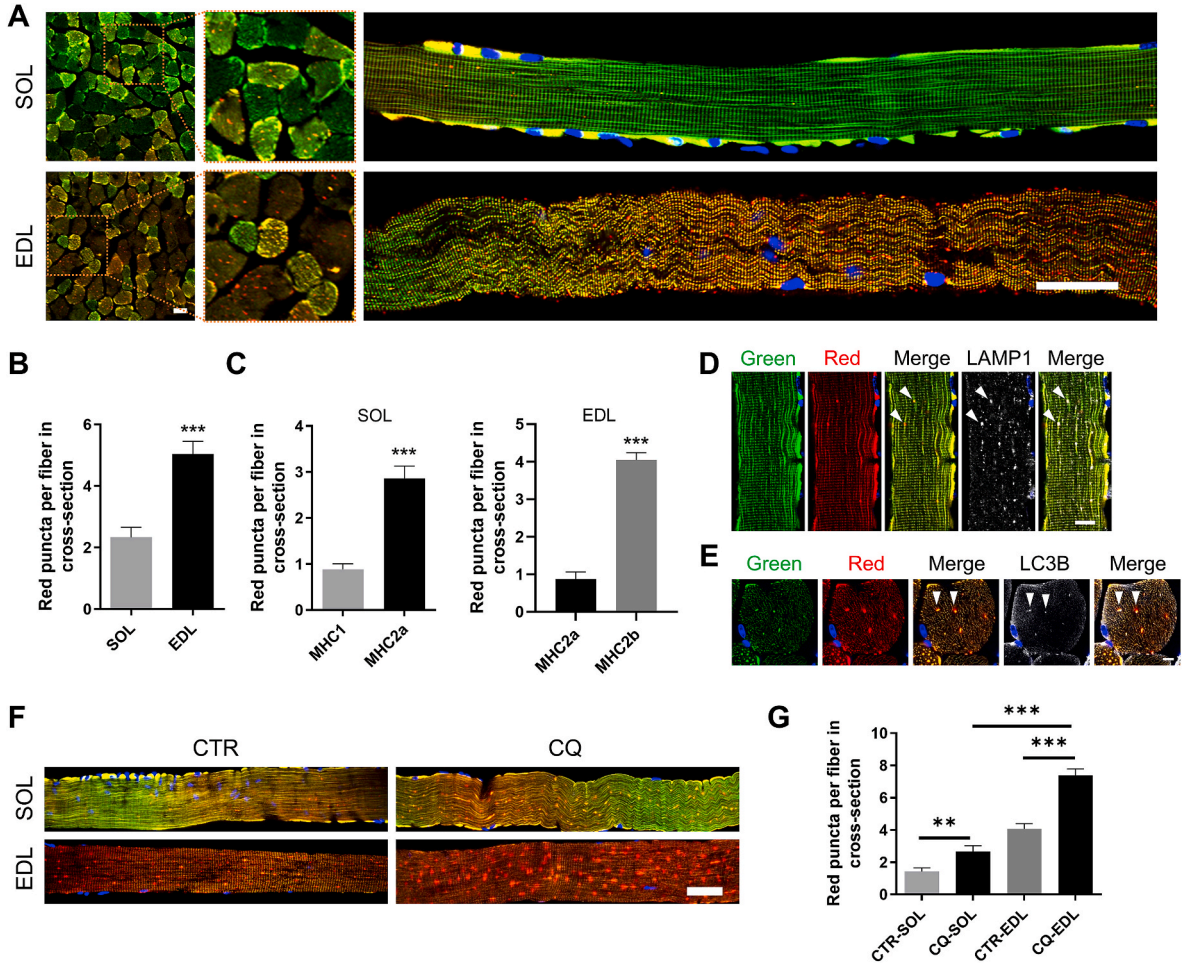

Fig. 3. The green predominant fluorescence spectrum of MitoTimer was not directly linked to selective mitophagy in the skeletal muscle fibers *in vivo*. (A) Representative fluorescence images of red puncta in soleus and EDL skeletal muscles and freshly isolated fibers. Scale bar, 50 μm. (B) Quantification of the red puncta in the cross-sections of single fibers from soleus and EDL muscles (69 fibers in cross-section counted in each group). (C) Quantification of the red puncta in the cross-sections of type 1, type 2A and type 2B fibers from soleus and EDL muscles (57–138 fibers in cross-section counted in each group). (D) Lamp1 immunofluorescence on muscle fibers showing co-localization with the red puncta. Scale bar, 20 μm. (E) LC3B immunofluorescence on muscle fibers showing co-localization with the red puncta. Scale bar, 10 μm. (F) Red puncta in soleus and EDL muscle fibers from control and CQ treated mice. Scale bar, 50 μm. (G) Quantification of the red puncta of single fiber in cross-section of soleus and EDL muscle from control and CQ treated mice (100–112 fibers in cross-section counted in each group). Data are presented as mean ± SEM. *$p < 0.05$, **$p < 0.01$, ***$p < 0.001$ (*t*-test). Representative results were shown from one mice. At least 3 mice were examined in each groups of the study. (For interpretation of the references to colour in this figure legend, the reader is referred to the Web version of this article.)

with limiting activities, the "older" proteins are more likely to be subjected to proteolysis than the newly synthesized proteins due to either simply their longer existence or possibly more damage sustained in their longer existence. Thus, the relative quantity of the "old" proteins as well as the ratio of "older" versus "young" proteins tends to reflect the protein degradation activity and dynamics under a homeostatic state. The observation that the oxidative metabolism linked green-predominant fluorescence spectrum of MitoTimer was commonly accompanied by a marked reduction in red fluorescence despite of unchanged or even increased green fluorescence (Fig. 2G and J and S3D) promoted us to examine MitoTimer protein degradation dynamics in different metabolic settings. MitoTimer-C2C12 myotubes were exposed to doxycycline for 24 h and chased for 6 h, 12 h, 24 h and 48 h in various culture media. MitoTimer protein level decreased at a faster rate in either the low glucose medium or the Galactose rich medium (Fig. 4A and S4A). A faster MitoTimer degradation under 2GAL culture condition was also evident in the MitoTimer-C2C12 myotubes with the treatment of protein synthesis inhibitor cycloheximide (CHX) (Fig. S4B).

To directly examine the mitochondrial proteolytic activity on MitoTimer in metabolically distinct cells, purified bacteria-expressed MitoTimer protein was incubated with the same amounts of mitochondrial extracts prepared from C2C12 cells with various culture media. Remarkably, MitoTimer was degraded faster in mitochondrial extracts from cells cultured in either low glucose or Galactose rich media (Fig. 4B and S4C). Importantly, the degradation of MitoTimer protein was more rapid in the mitochondrial extracts from soleus muscle compared to that from EDL muscle (Fig. 4C). These results indicated close links of the MitoTimer fluorescence spectrum, its degradation by the mitoproteolytic activity and the oxidative metabolic state. In addition, the respiratory complex I component NDUFB8 was also degraded faster in the mitochondrial extracts from cells cultured in the Galactose rich medium (Fig. S4D).

Mitoproteases are responsible for both the assembly of respiratory complexes and the degradation of misfolded, unassembled and oxidized proteins as part of the first line quality control system in mitochondria [9,32]. Lon protease homologue (LONP) and ATP-dependent Clp protease proteolytic subunit (CLPP) are the major mitoproteases for degradation of mitochondrial proteins in the matrix [9]. Knockdown of *Clpp* in the MitoTimer-C2C12 cells greatly increased MitoTimer protein accumulation (Fig. 4D) while knockdown of *Lonp1* moderately increased MitoTimer levels (Fig. S4E). Flow cytometry analysis found both a strong increase in the red fluorescence intensity and an increased red-to-green ratio in the knockdown cells (Fig. 4E–G and S4F–H), again indicating that the intensity of MitoTimer red fluorescence was intrinsically linked to the protein dynamics controlled by the mitoproteolytic activity. Notably, the knockdown of *Clpp* also increased the steady state level of NDUFB8 (Fig. 4D), consistent with its identification as a CLPP substrate [33,34], whereas the knockdown of *Lonp1* decreased the level of NDUFB8 (Fig. S4E), possibly due to its lack of assembly into the complex in the absence of LONP1 [35,36]. Consistently, the double knockdowns of both *Lonp1* and *Clpp* largely rescued the diminished NDUFB8 level in the mitochondrial extracts (Fig. S4I), supporting a major role of CLPP in the degradation of the unassembled respiratory complex subunit. To directly analyze the degradation of MitoTimer protein affected by CLPP and LONP1, MitoTimer protein was incubated with the mitochondrial extracts prepared from C2C12 cells with knockdown of *Clpp* and *Lonp1*. While knockdown of *Lonp1* had a minor effect on MitoTimer degradation by the mitochondrial extract, knockdown of *Clpp* significantly blocked MitoTimer degradation and knockdown of both *Clpp* and *Lonp1* completely abolished MitoTimer degradation (Fig. 4H). Thus, the degradation of MitoTimer protein was controlled by the mitoproteolytic system located in mitochondrial matrix.

The AAA proteases contain AAA modules responsible for ATP binding and hydrolysis [9,37,38]. To evaluate the energetic dependence in the degradation of MitoTimer protein, purified MitoTimer protein were incubated with extracts of mitochondria isolated from the mouse skeletal muscles with increasing amounts of ATP to a maximum concentration of 5 mM for 2 h. ATP strongly stimulated the degradation of MitoTimer in a dose dependent manner (Fig. 4I). Indeed, the green predominant mitochondria in cells under oxidative culture conditions all exhibited a higher level of mitochondrial ATP (Fig. 4J and K). When mitochondria from soleus muscle were pre-treated with oligomycin, which blocked mitochondrial ATP synthesis, the mitoproteolyticactivity of their extracts on MitoTimer was completely blocked (Figure 4L). Conversely, the inefficient degradation of MitoTimer in the mitochondrial extracts from EDL muscle was fully rescued with the pre-treatment of ATP (Figure 4M). Notably, the same amounts of mitochondrial extracts used for the mitoproteolytic assay contained comparable levels of CLPP protein from cells cultured in different media, and yet they exhibited striking differences in the mitoproteolytic activities when either directly or indirectly compared (Figs. S4J-K, 4B, S4C). Along this line, it is also worth noting that the increased mitochondrial ATP levels in the oxidative myotubes were also measured on a per-unit mitochondrial protein base, consistent with a highly efficient OXPHOS state. Collectively, these results indicated the energy level and its coupled enzymatic activity as a major determinant on the mitoproteolytic capacity and MitoTimer fluorescence spectrum.

Consistent with the coupling of MitoTimer fluorescence with the energy dictated mitoproteolytic activity, increasing cellular calcium concentration, which is known to increase oxidative metabolism and ATP generation [39], either by a brief $CaCl_2$ supplement in the culture medium or ionomycin treatment, resulted in a green predominant MitoTimer fluorescence spectrum in the MitoTimer-C2C12 myotubes (Figs. S5A–F). On the other hand, the treatment of either oligomycin or FCCP, which decouples the intermembrane H^+ gradient from ATP synthesis, resulted in a rapid accumulation of red fluorescence and a red predominant fluorescence spectrum within 6 h (Figs. S5G and H). Antimycin A, an inhibitor of the respiratory complex III, did not promote a significant shift of MitoTimer fluorescence spectrum by this time point (Figs. S5G and H). Indeed, the treatment of either oligomycin or FCCP, but not that of antimycin, reduced mitochondrial ATP level at 6 h (Fig. S5I). Interestingly, within the timeframe of the treatments, both cellular and mitochondrial ROS levels had not significantly altered (Figs. S5J and K), indicating a more direct link of MitoTimer fluorescence with the mitochondrial energy state, but not the redox state in this context. We also found the treatment of either the ROS scavenger NAC or H_2O_2 did not significantly affect MitoTimer fluorescence spectrum (Fig. S5L, M). By 24 h, the treatment of oligomycin, FCCP and antimycin all promoted a reduction of MitoTimer green fluorescence and a red predominant fluorescence spectrum (Fig. S5N, O), suggesting that the prolonged treatment of these mitochondrial inhibitors would lead to multiple alterations in the mitochondrial state. Nonetheless, besides other possible defects including that of mitochondrial import, a significant down-regulation of mitoproteolytic activities was also evident under such circumstances (Fig. 5P).

Collectively, with the *in vivo* observation of green-predominant MitoTimer fluorescence spectrum found in the oxidative muscles, these results further demonstrated that exquisitely depending on their energetic state, the oxidative skeletal muscle maintained higher mitoproteolytic activities compared to their glycolytic counterpart and promoted a fast turnover of MitoTimer protein, suggesting a metabolically regulated process of mitochondrial matrix protein clearance and quality control.

2.5. *MitoTimer fluorescence spectrum and mitoproteolytic activity were regulated by PGC-1α*

Peroxisome proliferator-activated receptor-γ coactivator-1α (PGC-1α) is a master transcriptional factor to stimulate oxidative metabolism in various cell types [40]. PGC-1α is expressed at higher levels in the oxidative muscles compared with the glycolytic muscles [41]. However,

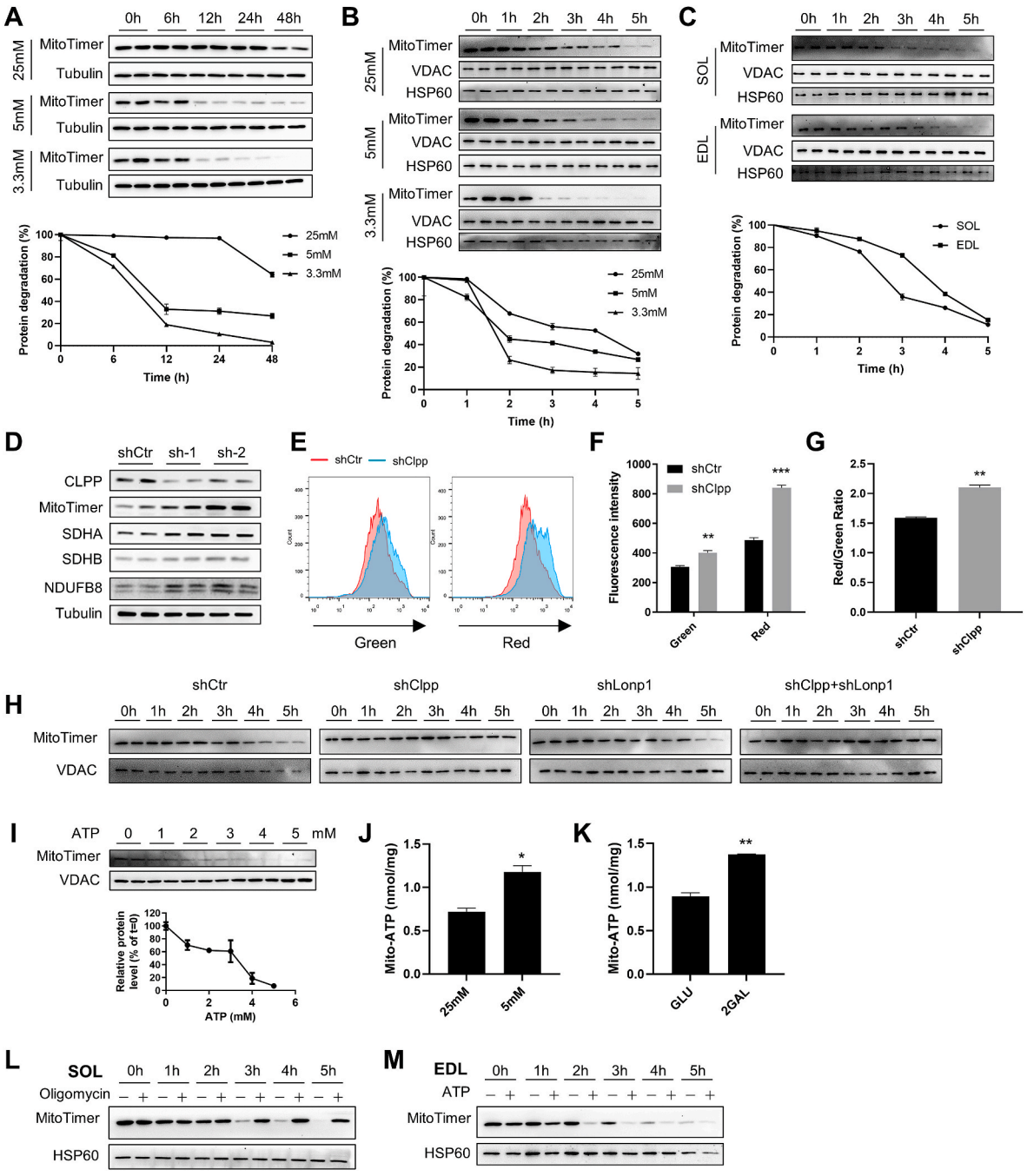

Fig. 4. Enhanced mitoproteolytic activities in cells and muscles with high OXPHOS activity. (A) Western blot analysis of MitoTimer proteins upon doxycycline withdraw at indicated time in MitoTimer-C2C12 myotubes treated with glucose-gradient media. (B) Western blot analysis of purified MitoTimer proteins incubated with mitochondrial extracts isolated from WT-C2C12 myotubes cultured in glucose-gradient media at indicated time. (C) Western blot analysis of purified MitoTimer proteins incubated with mitochondrial extracts isolated from soleus and EDL muscles of WT mice at indicated time. (D) Western blot analysis of MitoTimer, SDHA, SDHB and NDUFB8 expression in MitoTimer-C2C12 myoblasts with *Clpp* knockdown. (E) Flow cytometry analysis of MitoTimer fluorescence in MitoTimer-C2C12 myoblasts with *Clpp* knockdown. (F and G) Quantification of green and red fluorescence intensities and red/green fluorescence ratio by flow cytometry in MitoTimer-C2C12 myoblasts with *Clpp* knockdown. (H) Western blot analysis of purified MitoTimer proteins incubated with mitochondria extracts isolated from WT-C2C12 myoblasts with *Clpp* or *Lonp1* knockdown. (I) Western blot analysis of purified MitoTimer proteins incubated with mitochondria extracts isolated from skeletal muscle with dose ATP addition. (J) ATP level of mitochondria isolated from WT-C2C12 myotubes cultured in glucose-gradient media. (K) ATP level of mitochondria isolated from WT-C2C12 myotubes cultured in GLU and Gal-rich medium. (L) Western blot analysis of purified MitoTimer proteins incubated with mitochondria extracts isolated from WT soleus muscle with oligomycin (2 mM) treatment. Mitochondria were pre-treated with oligomycin at 25 °C for 20 min before sonication. (M) Western blot analysis of purified MitoTimer proteins incubated with mitochondria extracts isolated from WT EDL muscle with ATP (5 mM) addition. ATP was incubated with mitochondria at 25 °C for 20 min before sonication. Data are presented as mean ± SEM. *p < 0.05, **p < 0.01, ***p < 0.001 (*t*-test). (For interpretation of the references to colour in this figure legend, the reader is referred to the Web version of this article.)

whether PGC-1α is involved in regulating mitoproteolysis is unclear. Interestingly, the MitoTimer-C2C12 myotubes infected with adenovirus expressing PGC-1α exhibited a green-predominant MitoTimer fluorescent spectrum under the high glucose culture condition (Fig. 5A–C). Corroboratively, mitochondria isolated from these myotubes exhibited increased mitochondrial ATP generation and elevated mitoproteolytic activity (Fig. 5D and E), suggesting PGC-1α promoted the mitoproteolytic activity and qualitative alterations of the mitochondria functional state in addition to its role in mitochondrial biogenesis and expansion. In contrast, infection of adenovirus expressing *Pgc-1α* shRNA led to an increased abundance of MitoTimer protein, consistent with a down-regulation of the mitoproteolytic activity (Fig. 5F). Importantly, the green predominant fluorescence spectrum of the MitoTimer-C2C12 myotubes cultured in the Galactose rich or low glucose media exhibited a dramatic shift toward red with the knockdown of *Pgc-1α*, marked by a significant increase in the red fluorescence intensity (Fig. 5G and H).

PGC-1α promotes mitochondrial biogenesis under various contexts, which is important to increase the oxidative capacity of the cells [42–44]. Consistent with a qualitative difference of mitoproteolytic activities between the cells with distinct metabolic states (Fig. S6A), when we quantified the relative mitoproteolytic activity on MitoTimer and calculated the total mitoproteolytic activities taking into account the levels of mitochondrial protein isolated from the cells, we found the total mitoproteolytic activities were further increased in the cells under the oxidative condition, suggesting that the enhanced biogenesis under this condition only contributed to the increased total mitoproteolytic activities in the cells (Figs. S6A–C).We further investigated whether mitochondrial biogenesis, per se, would directly influence the read-outs on the measurements of the MitoTimer fluorescence spectrum and the mitoproteolytic activity. Similar to C2C12 myotubes, C2C12 myoblasts under the oxidative culture conditions also exhibited increased biogenesis and oxidative metabolism as evidenced by the increased respiratory complex expression (Fig. S6D), mtDNA/nDNA ratio (Fig. S6E) and oxygen consumption (Fig. S3A). However, in contrast to the myotubes, these cells did not exhibit elevated mitochondrial ATP levels (Fig. S6F), indicating a decoupling of OXPHOS with oxygen consumption and mitochondrial biogenesis possibly due to the cells' anabolic nature. Interestingly, the C2C12 myoblasts under the oxidative conditions did not exhibit alterations in their MitoTimer fluorescence spectrum and mitoproteolytic activities on MitoTimer (Figs. S6G–I), strongly suggesting that enhancing mitochondrial biogenesis had no

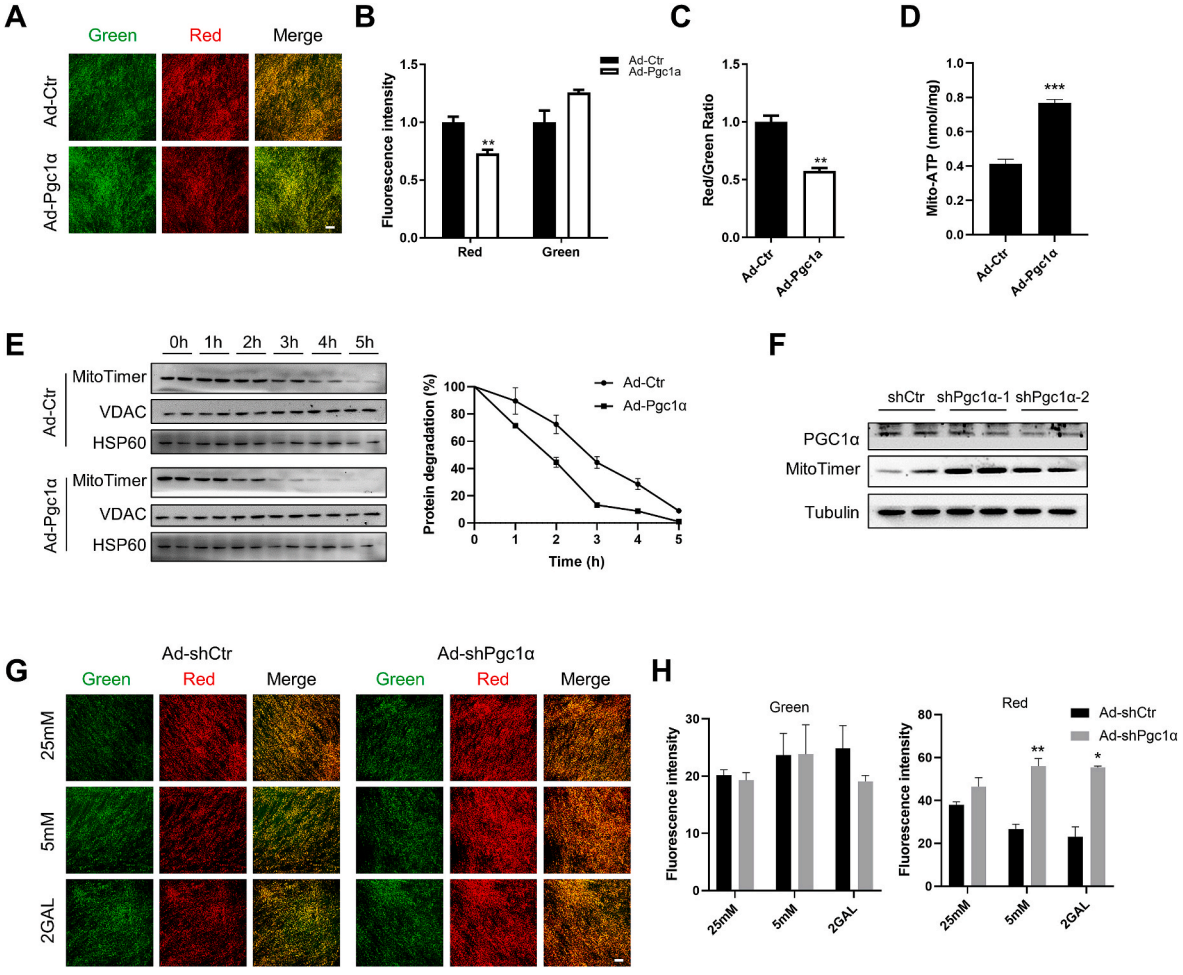

Fig. 5. MitoTimer fluorescence spectrum and mitoproteolytic activity were regulated by PGC-1α. (A) Images of MitoTimer fluorescence in MitoTimer-C2C12 myotubes infected with adenoviral *Pgc-1α*. Scale bar, 200 μm. (B, C) Quantifications of green and red fluorescence intensities (B) and their ratios (C) in MitoTimer-C2C12 myotubes infected with adenoviral *Pgc-1α*. (D) ATP level of mitochondria isolated from WT-C2C12 myotubes infected with adenoviral *Pgc-1α*. (E) Western blot analysis of purified MitoTimer proteins incubated with mitochondrial extracts isolated from WT-C2C12 myotubes infected with adenoviral *Pgc-1α* at indicated time. (F) Western blot analysis of MitoTimer expression in MitoTimer-C2C12 myotubes infected with adenoviral *shPgc-1α*. (G) Images of MitoTimer fluorescence in MitoTimer-C2C12 myotubes infected with adenoviral *shPgc-1α* and cultured in GAL-rich or low glucose medium. Scale bar, 200 μm. (H) Quantifications of green and red fluorescence intensities in MitoTimer-C2C12 myotubes infected with adenoviral *shPgc-1α* and cultured in GAL-rich or low glucose medium. Data are presented as mean ± SEM. *p < 0.05, **p < 0.01, ***p < 0.001 (*t*-test). (For interpretation of the references to colour in this figure legend, the reader is referred to the Web version of this article.)

major obligatory effect on the readouts of either MitoTimer fluorescence or its degradation. In addition, the C2C12 myotubes with the knock-down of *Clpp*, while still undergoing active biogenesis under the oxidative culture condition, significantly accumulated MitoTimer red fluorescence, again indicating that the MitoTimer red fluorescence was strongly dependent on its degradation, but not other factors (Fig. S6J-L).

Together, these results substantiated a critical role of PGC-1α in coordinately regulating OXPHOS and mitoproteolysis, and further supported the notion that high OXPHOS levels underlay the enhanced mitoproteolytic activity and green predominant fluorescence spectrum of MitoTimer.

2.6. Anti-ageing agents involved in the nutrient sensing pathways promoted active oxidative phosphorylation

Our finding of the green predominant mitochondrial state in the low glucose culture medium indicated a role of the nutrient sensing and the Sirtuin pathway in regulating mitoproteolysis. As a cofactor for Sirtuin activity, NAD^+ and its metabolism links cell metabolic state to cellular defense against oxidative stress [45]. Interestingly, Nicotinamide Riboside (NR), a precursor for NAD^+ synthesis, also promoted a rapid increase in mitochondrial ATP generation (Fig. 6A) and a shift to a green predominant MitoTimer fluorescence spectrum (Fig. 6B–D). The effect was SIRT1 dependent as its inhibition by EX527 resulted in a reduction of mitochondrial ATP level and a shift to a red predominant fluorescence spectrum of MitoTimer (Fig. 6A–D). The treatment of AZD2281, another booster of NAD^+ levels, promoted a green predominant MitoTimer fluorescence spectrum similarly with NR (Figs. S7A–C). AZD treatment also resulted in increased mitoproteolytic activity (Fig. S7D). Consistent with the role of SIRT1 in deacetylating and activating PGC-1α, knock-down of *Pgc-1α* in the NR treated MitoTimer-C2C12 myotubes led to a shift to red predominant fluorescence spectrum (Fig. 6E–G), suggesting that these agents may promote the active mitochondrial state in a PGC-1α dependent manner. Along this line, a low dose of rapamycin treatment, known to promote PGC-1α expression [46,47], also led to an elevated mitochondrial ATP production and a green predominant MitoTimer fluorescence spectrum in the C2C12 myotubes (Fig. 6H–K).

The tight coupling of enhanced mitoproteolysis with oxidative phosphorylation and ATP production suggested a highly stringent quality control mechanism and promoted us to examine the redox state of the green predominant MitoTimer expressing cells. The cells cultured in either Galactose rich or low glucose media, or under NR treatment, all exhibited elevated TMRM (Fig. 6L, M) and NAD^+/NADH levels (Fig. 6N, O), as well as enhanced mitochondrial respiratory complex activities (Figs. S7E and F). The mitochondria in soleus muscle also exhibited enhanced respiratory complex III activity compared with that from the EDL muscle (Fig. S7G). Meanwhile, cells with the green predominant MitoTimer fluorescence also exhibited reduced protein carbonylation (Fig. 6P, Q) and lower MitoSOX levels (Fig. 6R, S), together with increased expression of nuclear factor erythroid 2-related factor 2 (NRF2) and FOXO3a (Figs. S7H and I), indicating an elevated defense against oxidative damage. Importantly, by blue-native polyacrylamide gel-electrophoresis (BN-PAGE) analysis, the "green predominant" mitochondria possessed increased amounts of the respiratory supercomplexes (Fig. 6T, U), known to facilitate more fluent electron transfers between the complexes [48,49]. Thus, the "green predominant" mitochondria with the high mitoproteolytic activity represented a metabolically active, highly energetic and well protected population under various contexts.

Finally, the oxidative culture conditions were able to promote a green predominant MitoTimer fluorescence spectrum in confluent MEFs (Fig. S7J-L). We also observed a distinct green predominant MitoTimer fluorescence spectrum in the villi compared with that in the crypt of the small intestine of the dMT mice (Fig. S7M), paralleling the distinct metabolic states in the differentiated cell versus stem cell compartments. These results suggested that besides skeletal muscle, MitoTimer fluorescence spectrum and possibly mitoproteolysis may also be subjected to the metabolic regulation in other types of cells and tissues.

3. Discussion

The quality control for mitochondria plays fundamental roles not only in mitochondria health, but in the integrity and functional fitness of tissues and organisms. The mitochondrial proteostasis represents the first line quality control mechanisms that safeguard mitochondria integrity and function. Stimulated by *in vivo* observations from the MitoTimer reporter, we found the mitochondrial matrix proteolytic activity was elevated in the oxidative cells and tissues and promoted by the Sirtuin/PGC-1α axis, substantiating a tight coupling of mitoproteolysis and oxidative phosphorylation. Importantly, the cells with active mitoproteolysis are highly protected from oxidative stress, reminiscent of the prominent role of enhanced mitoUPR in the longevity of C. *elegans* [50].

MitoTimer fluorescence spectrum has been found to be influenced by many factors and the nature of its *in vivo* heterogeneity and alteration remains elusive [23,24]. It was proposed that the changes in MitoTimer green fluorescence suggested possible variations in mitochondrial protein synthesis, import and biogenesis, while the changes in MitoTimer red fluorescence may reflect alterations in mitochondrial degradation [23], but no direct proof was provided, especially under physiological contexts. Here we found that for a general population of mitochondria in a given cell, the overall MitoTimer fluorescence spectrum, especially the relative red fluorescence, was greatly influenced by the mitoproteolytic activity and its tight coupling with the oxidative metabolism and energetic state. These results should facilitate further understanding of the existing diverse observations on MitoTimer fluorescence spectrum. Indeed, a plethora of factors and processes that were reported to alter MitoTimer fluorescence spectrum apparently impacted the mitochondrial oxidative metabolism [21,22,51]. Further studies are warranted to interpret these observations in the direction of cellular metabolic regulation and heterogeneity. Other quality control mechanisms including mitophagy may also directly influence MitoTimer fluorescence spectrum [52], possibly under stress situations when mitochondrial homeostasis was severely disturbed.

While our results indicated a major role of mitoproteolysis in determining MitoTimer fluorescence spectrum through the differential degradation dynamics of the green and red MitoTimer proteins, a mathematical model of time-associated differential protein degradation dynamics for the "old" versus "young" Timer proteins would be idealto ultimately prove the influence of mitoproteolytic activity on the MitoTimer fluorescence spectrum. A reporter that exclusively reflects the level of mitoproteolysis could also be designed and utilized to directly measure the mitoproteolytic activities. Other mechanisms such as mitochondrial import might help to explain the diversity of MitoTimer fluorescence intensities observed in addition to the red/green ratios [21,23]. We indeed observed an increase in the green fluorescence intensity under some oxidative conditions without a proportional increase in the red fluorescence (e.g. Figs. S3B–D). Conversely, relatively longer treatment of mitochondrial inhibitors resulted in a significant decrease in the green fluorescence without a proportional decrease in the red fluorescence (e.g. Fig. S5N). These disproportional changes of MitoTimer green and red fluorescence might reflect combinatorial effects of mitoproteolysis and mitochondrial import, which requires further investigation.

By elucidating the nature of a general pattern of the green predominant MitoTimer fluorescence, we further addressed the fundamental features of a "healthy" mitochondrial functional state with reduced oxidative stress as elegantly proposed by Laker et al. [22]. Our finding that the green predominant MitoTimer fluorescence is greatly influenced by the mitoproteolytic activity and mitochondrial energetic state emphasized a unique active mitochondrial state with enhanced OXPHOS and tightened quality control/antioxidant defense mechanisms. Whether the redox state or its controlling mechanisms may also directly

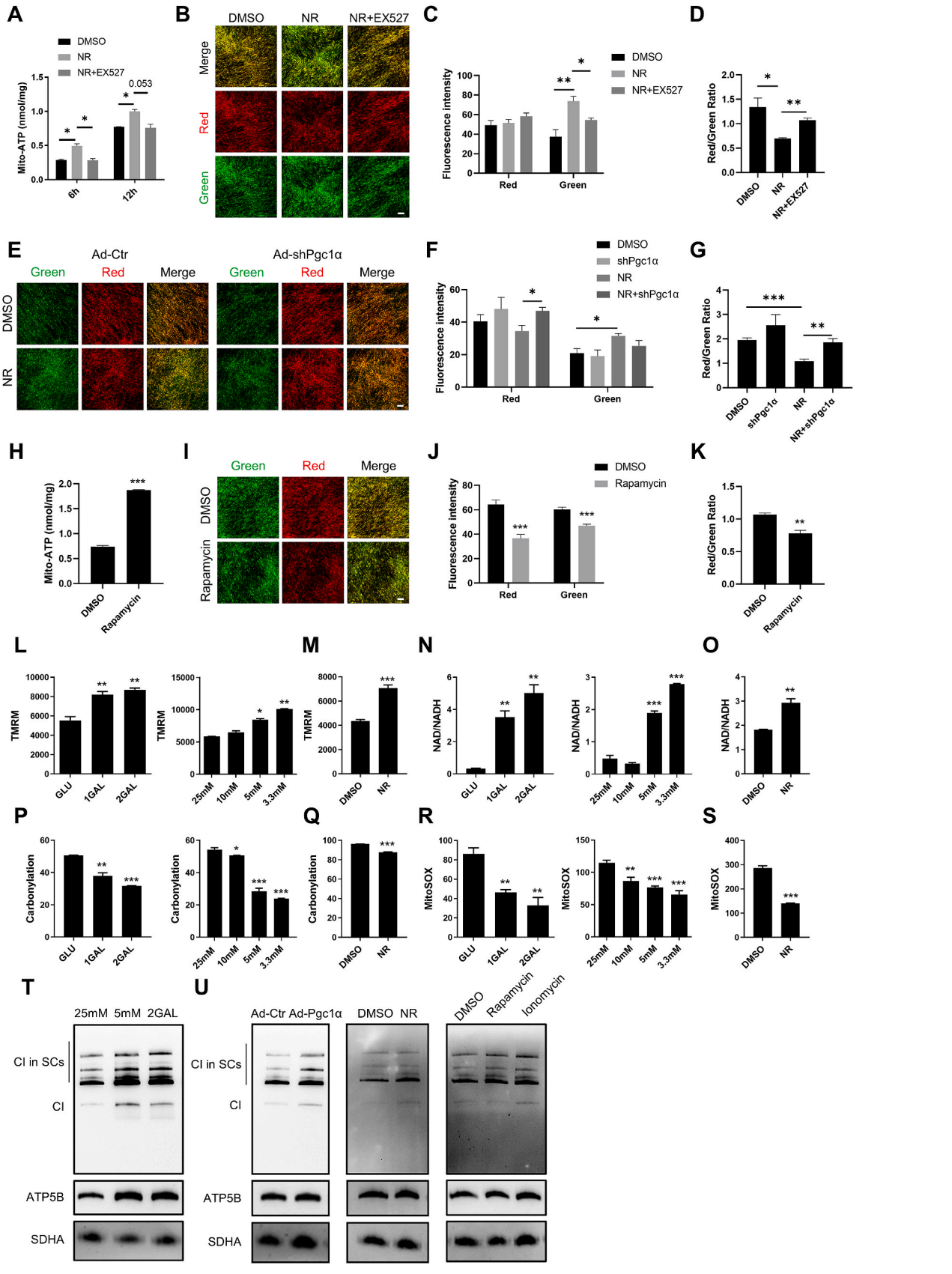

(caption on next page)

Fig. 6. Anti-ageing agents promoted both mitoproteolysis and active oxidative metabolism. (A) ATP level of mitochondria isolated from WT-C2C12 myotubes treated with DMSO or NR (1 mM) and SIRT1 inhibitor EX527 (20 μM) at indicated time. (B) Images of MitoTimer fluorescence in MitoTimer-C2C12 myotubes treated with DMSO or NR (1 mM) and EX527 (20 μM) for 48 h. Scale bar, 200 μm. (C, D) Quantifications of green, red fluorescence intensities (C) and their ratios (D) in MitoTimer-C2C12 myotubes treated with DMSO or NR (1 mM) and EX527 (20 μM) for 48 h. (E) Images of MitoTimer fluorescence in MitoTimer-C2C12 myotubes infected with adenoviral *shPgc-1α* under the treatment of DMSO or NR (1 mM) combining. Scale bar, 200 μm. (F, G) Quantifications of green, red fluorescence intensities (F) and their ratios (G) in MitoTimer-C2C12 myotubes infected with adenoviral *shPgc-1α* under the treatment of DMSO or NR (1 mM) combining. (H) ATP level of mitochondria isolated from WT-C2C12 myotubes treated with DMSO or rapamycin (1 nM) for 48 h. (I) Images of MitoTimer fluorescence in MitoTimer-C2C12 myotubes treated with DMSO or rapamycin (1 nM) for 48 h. Scale bar, 200 μm. (J, K) Quantifications of green, red fluorescence intensities (J) and their ratios (K) in MitoTimer-C2C12 myotubes treated with DMSO or rapamycin (1 nM) for 48 h. (L, M) TMRM levels of WT-C2C12 myotubes cultured in GAL-rich or low glucose medium or treated with NR (1 mM). (N, O) NAD/NADH ratio of WT-C2C12 myotubes cultured in Gal-rich or low glucose medium or treated with NR (1 mM). (P, Q) The protein carbonylation levels of WT-C2C12 myotubes cultured in GAL-rich or low glucose medium or treated with NR (1 mM). (R, S) MitoSOX levels of WT-C2C12 myotubes cultured in GAL-rich or low glucose medium or treated with NR (1 mM). (T) Immunodetection of the indicated proteins representing CI, CII and CV after blue native PAGE (BN-PAGE) of digitonin-solubilized mitochondria from WT-C2C12 myotubes cultured in GAL-rich or low glucose medium. (U) Immunodetection of the indicated proteins representing CI, CII and CV after BN-PAGE of digitonin-solubilized mitochondria from WT-C2C12 myotubes infected with adenoviral *Pgc-1α* or treated with NR (1 mM), rapamycin (1 nM) or ionomycin (0.5 μM). Data are presented as mean ± SEM. *p < 0.05, **p < 0.01, ***p < 0.001 (*t*-test). (For interpretation of the references to colour in this figure legend, the reader is referred to the Web version of this article.)

influence MitoTimer fluorescence, per se, remains not completely understood. With the treatment of mitochondrial inhibitors, a rapid accumulation of MitoTimer red fluorescence is accompanied by ATP depletion without any changes in the ROS levels. On the other hand, it would be interesting to investigate the action of some antioxidants in promoting oxidative metabolism under certain circumstances. Collectively, our study represents a significant advance in the utilization of MitoTimer as an important probe for an active mitochondrial OXPHOS state. Although MitoTimer fluorescence spectrum mainly indicated the activity of CLPP/LONP1 and the mitochondrial energetic state under various contexts, the ATP dependent nature of multiple mitoproteases strongly suggested that the mitoproteolysis as a whole were coordinately regulated with the OXPHOS activity. Thus, this study also emphasized an intrinsic regulation of mitoproteolysis under physiological context. The increased mitochondrial ATP production promoted the energetic coupling of mitoproteolytic activities and represented a critical layer of regulation to safeguard OXPHOS with a feed-forward mechanism.

The apparent coordination of mitoproteolysis and oxidative metabolism by Sirtuin/PGC-1α axis underlying the green predominant mitochondrial state may provide an integrative framework for understanding the critical requirements in the promotion and maintenance of an active mitochondrial respiration and oxidative phosphorylation. Besides biogenesis, there is growing evidence that PGC-1α also modulates the intrinsic composition of mitochondria beyond the quantitative increase [40,42,44]. Our results also indicated regulations beyond mitochondrial biogenesis dictated the mitoproteolytic activity. In addition to its role in the clearance of damaged proteins, mitoproteostasis also participates in the correct processing, folding, sorting, assembly and remodeling of the respiratory complex proteins [9]. Our finding of a comprehensive integration of mitoproteolysis in the oxidative metabolism strongly supported its key role in facilitating OXPHOS while preventing oxidative damage by the promotion of both the assembly of functional complexes and the clearance of the unassembled and damaged proteins. Along this line, as other mitoproteases including YME1L, play critical roles controlling mitochondrial dynamics and cristae remodeling [53], their activation may lead to elongated mitochondria with highly compacted mitochondrial cristae, facilitating the increases in mitochondrial respiratory complex activity and supercomplex formation found in the green predominant mitochondria, features of which are closely associated with increased OXPHOS efficiency and reduced electron leaks [48,49].

The metabolic [$^2H_3$]-leucine isotope labeling indicated that mitochondrial respiratory chain protein complexes turned over in a heterogeneous fashion [54]. The higher mitochondrial proteolytic activities we found in the oxidative muscle fibers may ensure timely replacements of respiratory chain proteins and allow efficient OXPHOS, highly consistent with the report that mitochondrial protein turnover faster in soleus muscle than EDL [55]. In this regard, our study suggest that the green predominant mitochondria did not necessarily represent the “new” or “young” mitochondria per se, rather, they represented highly active mitochondria with a faster protein turnover compared with the less active mitochondria in the glycolytic cells. Moreover, the active mitoproteolysis, while helping to sustain the OXPHOS activity, was distinct from a macro degradation process such as mitophagy which was actually attenuated in the soleus muscle (Fig. 3B), although the basal level of mitophagy was still essential for tissue homeostasis [31,56,57]. Mitochondrial quality control mechanism might be functional at multiple levels to govern mitochondrial health [6,58]. As the mitochondrial energetic state may influence the choice of mitophagy [59,60], the differential regulation of mitoproteolysis and mitophagy in the metabolically distinct muscle fibers highlighted the energy dependent determination of these quality control mechanisms.

Finally, this study helps to pinpoint the underlying essence of metabolic fitness. The enhanced OXPHOS coupled with stringent quality control mechanisms may also engage in other redox controlling mechanisms to promote an ideal state for meeting both the energy demand as well as self-maintenance requirements. Indeed, the oxidative muscle fiber is better maintained than the glycolytic fiber during ageing [61], while endurance exercise, known to increase the oxidative capacity of skeletal muscles, helps to protect from ageing associated muscle weakness and atrophy [62,63]. Given the multiple beneficial effects of NR and many possible mechanisms involved [14], we revealed mechanistic insight of NR in possibly coordinately promoting oxidative metabolism and mitoproteolysis. How the multiple quality control and redox controlling pathways are intertwined to determine or maintain an active mitochondrial state and a favorable cellular outcome is an extremely interesting question to address in the future. In this perspective, the MitoTimer system can be manipulated to accelerate the discovery of novel drugs aiming to elevate mitochondrial bioenergetics while countering oxidative damage.

The nutrient and metabolic sensing mechanisms by Sirtuin, AMPK, mTOR and others play prominent roles in controlling organismal health and longevity [45,64]. The convergence of these pathways with mitoproteostasis and oxidative metabolism in mammalian systems as revealed in this study should have broad implications in understanding and treating ageing and ageing associated diseases.

4. Materials and methods

4.1. Mouse generation and animal care

The MitoTimer cDNA was cloned from plasmid derived from addgene (#52659). pRosa-CAG-rtTA-TRE-LSL-MitoTimer plasmid was generated by removing the GFP-WPRE cDNA from the pRosa-CAG-rtTA-TRE-LSL-GFP plasmid by *EcoRV* and inserting the MitoTimer cDNA and WPRE fragments into the pRosa backbone through homologous recombination. pRosa-CAG-rtTA-TRE-LSL-MitoTimer plasmid have 5′ and 3’ homologous recombination arms of the *ROSA26* BAC. The

linearized pRosa-CAG-rtTA-TRE-LSL-MitoTimer plasmid digested by *AscI* was electrically transferred to DY380 competent cells to achieve homologous recombination into the *ROSA26*BAC. The linearized *ROSA26*-MitoTimer BAC was microinjected into the male pronucleus of the mouse zygotes. MitoTimer (MT) BAC transgenic mice were created in Model Animal Research Center with C57BL/6J and CBA mixed background and were backcrossed to C57BL/6J background. MT mice were crossed to EIIa-Cre mice to delete "STOP" cassette (dMT). Primers for genotyping are listed in Supplementary Table 1.

For chloroquine (CQ) treatment, 2–3 months old dMT mice were administered intraperitoneally with 50 mg/kg/day dose of chloroquine diphosphate in PBS or PBS for 3 consecutive days. Mice were sacrificed 4 h after the last chloroquine dose.

Mice were bred and maintained under specific pathogen-free conditions in a controlled environment of 20–22 °C, with a 12/12 h light/dark cycle. Food and water were provided ad libitum. All animal experiments were approved by the Institutional Animal Care and Use Committee (IACUC) of Model Animal Research Center, Nanjing University, China.

4.2. Tissue preparation and confocal microscopy

Fresh tissues were removed from mouse and fixed in ice-cold 4% PFA for 2–6 h. Fixed tissues were washed in PBS three times, 5 min each, before density-dependent cryoprotection in 30% sucrose at 4 °C overnight. Cryoprotected tissues were embedded in OCT and frozen via liquid nitrogen. Tissues were stored at −80 °C until used or immediately sectioned. The tissues were sliced into 10 μm-size sections on a cryostat. The sections were mounted on slides. For an alternative method of tissue preparation, the harvested soleus and EDL were immediately fixed in 4% paraformaldehyde for 20 min and mounted in 50% glycerol in phosphate buffered saline with coverslips on gelatin-coated glass slides for imaging [51].

For single skeletal muscle fiber isolation, EDL and soleus muscles were dissected from the mouse hindlimb. Then straightened muscles were fixed with 4% paraformaldehyde (PFA) on ice for 1 h. After fixation, muscles were washed with ice-cold PBS twice, 3 min each. The tendon and connective tissue of muscles were cleared under microscope. Then single muscle fibers were carefully separated with microscopic tweezers and place them on the slides. The separated muscle fibers were mounted with anti-fading VECTASHIECD mounting medium with DAPI (Vector). For mitochondrial morphological resolution of skeletal muscle, the extensor digitorum longus (EDL) and the tibialis anterior (TA), both fast-twitch muscles, were observed with small block-like mitochondria arranged in rows and columns when viewed along the long axis of the fiber. Soleus and diaphragm, two slow-twitch muscles, were observed with partially continuous longitudinal rows that span mitochondria from multiple sarcomeres [18].

For immunofluorescence analysis, frozen sections were rinsed with PBS three times, 3 min each, and then blocked with 10% goat serum for 30–60 min at room temperature. The serum-blocked slides were then incubated with primary antibodies at 4 °C overnight. After triple washing with PBS, 3 min each, the slides were incubated with mixture of DAPI and fluorescent compound-tagged secondary antibodies at room temperature for another 2 h. Finally, the slides were washed with PBS three times, 5 min each, and mounted in 50% glycerol in PBS to analyze with a confocal microscope.

For MitoTimer imaging, sections were analyzed with Olympus FV1000 laser confocal microscopic imaging system using the green (excitation/emission 488/518 nm) and red (excitation/emission 543/572 nm) channels. To control for possible bleaching during multiple acquisitions, the laser parameters were set to the minimal level. Resulting images in one group for analyzing the fluorescence intensity of red, green, and the red/green ratio, all samples were guaranteed to be photographed with identical predetermined acquisition parameters at one time. Image J was used to quantify green and red fluorescence intensity of the images.

4.3. Tissue culture and cell line generation

MEFs and C2C12 myoblasts were cultured with Dulbecco's Modified Eagle's Medium (DMEM, Gibco, Catalog #12800) supplemented with 10% FBS, and penicillin/streptomycin under 5% CO2 at 37 °C for routine culture. For C2C12 differentiation, C2C12 myoblasts were cultured to 100% confluence and switched to differentiation medium consisting of DMEM containing 2% horse serum and penicillin/streptomycin for 3–5 days.

For medium induced cell metabolic alteration in C2C12 myotubes, GLU media were prepared by the base DMEM (Gibco, Catalog #A14430) supplemented with 2% horse serum, 10 mM glucose, 4 mM glutamine, and penicillin/streptomycin. 1GAL (1ACE) media were prepared by the base DMEM supplemented with 2% horse serum, 6.7 mM glucose, 3.3 mM galactose (acetoacetate), 4 mM glutamine, and penicillin/streptomycin. 2GAL (2ACE) media were prepared by the base DMEM supplemented with 2% horse serum, 3.3 mM glucose, 6.7 mM galactose (acetoacetate), 4 mM glutamine, and penicillin/streptomycin. Glucose-gradient media were prepared by the base DMEM supplemented with 2% horse serum, indicated glucose concentration, 4 mM glutamine, and penicillin/streptomycin. For MEFs and C2C12 myoblasts, glucose-gradient media were prepared by the base DMEM supplemented with 10% FBS, indicated glucose concentration, 4 mM glutamine, and penicillin/streptomycin. GLU media were prepared by the base DMEM supplemented with 10% FBS, 10 mM glucose, 4 mM glutamine, and penicillin/streptomycin. 1GAL media were prepared by the base DMEM supplemented with 10% FBS, 6.7 mM glucose, 3.3 mM galactose, 4 mM glutamine, and penicillin/streptomycin. 2GAL media were prepared by the base DMEM supplemented with 10% FBS, 3.3 mM glucose, 6.7 mM galactose, 4 mM glutamine, and penicillin/streptomycin. MEFs were seeded with different densities (the cell density ratio was 1:3). When the cultured wells in plate with densely plated were full of cells, inducible media were exchanged. Sparsely plated wells were changed with glycolytic media and the densely plated wells were changed with oxidative media. For media exchanges, cells were washed three times with the indicated media.

C2C12 cells were seeded into 6-well plates one day prior to transfection at a density of about 50%. Cells were transfected with 3 μg pRosa-CAG-rtTA-TRE-MitoTimer-Neo plasmid using Lipofectamine 3000 (Life Technologies) following the manufacturer's recommended protocol. 24 h after the transfection, the cells were treated with G418 (HyClone) at the final concentration of 400 μg/mL for 10 days for positive selection. Then the cells were treated with doxycycline at the concentration of 1 μg/mL to induce MitoTimer expression either before or after being picked as clones into 96-well plate.

For MitoTimer fluorescence analysis, MitoTimer-C2C12 myotubes were cultured for 4days in GAL-rich or low glucose medium, with 1 μg/mL doxycycline treatment for 2days and then analyzed with BioTek Synergy H1 microplate reader or Olympus FV1000 laser confocal microscopic imaging system using the green (excitation/emission 488/518 nm) and red (excitation/emission 543/572 nm) channels.

4.4. Reagents

Antibodies used are listed in Supplementary Table 2. Nicotinamide Riboside chloride (MedKoo Biosciences, #329479), EX527 (Selleck, S1541), AZD2281 (APExBIO, A4154), metformin (Sigma, PHR1084), ionomycin (Selleck, S7074), rapamycin (Selleck, S1039), Bafilomycin A1(Selleck, S1413), Oligomycin (Millipore, 3433895), FCCP (Selleck, S8276) and Antimycin A1 (MedChemExpress, HY-107406) were used at indicated concentration.

4.5. Isolation of mitochondria

For mitochondria isolation from muscles, the muscles were cut into pieces in a homogenizing buffer (MIM buffer: 0.3 M sucrose, 10 mM HEPES and 0.2 mM EDTA, pH 7.2) and grinded using a homogenizer. For mitochondria isolation from cultured cells, C2C12 myotubes in 10 cm dish were collected and homogenized. The homogenized extract was then centrifuged twice for 5min at 600×*g* at 4°Cto obtain supernatant. Mitochondria were pelleted by centrifugation at 9000×*g* for 10 min at 4°Cto enrich for mitochondria and then washed twice with the same buffer.

4.6. MitoTimer protein purification and degradation assay

MitoTimer cDNA was PCR amplified, digested and subcloned into *Kpn*I and SmaIsites of pQE-30 vector containing an N-terminal 6 × His tag. The *E. coli* BL21 (DE3) cells were used for protein expression. The purification was performed following the protocol provided by manufacturer (Ni-NTA-Sefinose™ Resin, Sango Biotech, C600332).

Purified MitoTimer protein (2 μg) mixed with sonicated mitochondria (100 μg) in MIM buffer were divided equally into twelve tubes and incubated for 0~5 h at 37 °C (two duplicates), respectively. To test the effect of ATP on degradation of mitochondrial proteins, 100 μg isolated mitochondria in MIM buffer supplied with 5 mM ATP or 2 mM oligomycin were incubated at 25 °C for 20 min, and then sonicated. Purified MitoTimer protein (2 μg) mixed with the sonicated mitochondria (control or treated group) were divided equally into six tubes and incubated for 0~5 h at 37 °C, respectively. For cycloheximide (CHX) treatment, MitoTimer-C2C12 myotubes were cultured for 4days in GAL-rich medium, with 1 μg/mL doxycycline induction for 2days and the treatment of 20 μg/mL CHX for the final 8 h.

4.7. Flow cytometry

MEFs or C2C12 cells were harvested by brief trypsinization, followed by neutralization of trypsin, washing, and fixation within 4% paraformaldehyde in PBS. For mitochondrial FACS, the isolated mitochondria were fixed within 4% paraformaldehyde in PBS and washed with MIM buffer. The BD FACS AriaIII was used for analysis by 488-nm and 561-nm laser for excitation, FITC (green) and PE (red) channels for detection. Data were analyzed using FlowJo_V10 software.

4.8. RNA extraction and real-time RCR

Total RNA samples were isolated using TRIzol (Takara) and were reverse transcribed to cDNA following the manufacturer's instruction of Primescript™ RT reagent kit with gDNA eraser (Takara). Diluted cDNA was used for Real-time PCR with SYBR Green reagent (Roche) on ABI Prism Step-One bio-analyzer. Melt curves of specific primers were examined to confirm their specificities. Sequences of primers are listed in Supplementary Table 1. Expression data were normalized to 36b4 or Tbp expression. Expression changes were calculated using the ΔΔCt method and expressed as fold change over control.

4.9. Western blot

Samples were lysed in RIPA buffer with complete Protease Inhibitor Cocktail Tablets (Roche). Supernatant protein concentration was determined by PierceTM BCA Protein Assay kit (Thermo). Proteins were electrophoretically separated and immunoblotted onto polyvinylidene fluoride membranes. Membranes were incubated at 4 °C for 16 h with indicated primary antibodies and subsequently at room temperature for 2 h with horseradish-peroxidase-conjugated secondary antibodies. Detection was carried out with High-sig ECL (Tanon), and signals were visualized by a gel documentation system (Syngene). Protein bands were quantified by densitometry using Image J. The antibodies are listed in Supplementary Table 2.

4.10. Cellular metabolic and redox state measurements

Oxygen consumption was measured using a Seahorse XF24 Extracellular Flux analyzer (Seahorse Bioscience). Cells were cultured in 24-well Seahorse plates. Cell culture medium was replaced with XF-DMEM medium containing 2 mM L-glutamine, 2 mM sodium pyruvate and 25 mM glucose. Oxygen consumption was measured and respiration rate was analyzed with injections of 1 μM oligomycin, 1.5 μM FCCP and 1 μM antimycin A & rotenone (Seahorse Bioscience). Results were normalized to total protein determined using PierceTM BCA Protein Assay kit (Thermo).

The ATP levels of mitochondria were measured using a firefly luciferase-based ATP assay kit (Beyotime), according to the protocol provided by the manufacturer. Freshly prepared mitochondria were lysed and centrifuged at 12,000×*g* for 5 min. Supernatants (20 μl) and standards were mixed with 100 μl ATP detection working dilution in a 96-well plate at room temperature. The luminescence was measured using microplate reader (BioTek Synergy H1). The protein concentration of each treatment group was determined using the Pierce BCA Protein Assay Kit (Thermo). The total ATP levels were expressed as nmol/mg protein. Mitochondrial superoxide was detected by incubating C2C12 myotubes with 5 μM MitoSOX-Red (Invitrogen, excitation/emission at 510nm/580 nm) for 10 min at 37 °C using microplate reader (BioTek Synergy H1). For TMRM measurement, C2C12 myotubes were pre-incubated with tetramethylrhodamine methyl ester (TMRM) (Invitrogen) for 30 min at 37 °C and detected at excitation/emission at 530nm/580 nm using microplate reader (BioTek Synergy H1). Protein carbonyl concentration was determined in C2C12 myotubes using a Protein Carbonyl Content Assay Kit (Sigma-Aldrich, MAK094) and following the manufacturer's instructions. The amount of protein carbonyl in each sample was reported as nmol protein carbonyl per mg total protein. The protein concentration of each treatment group was determined using the Pierce BCA Protein Assay Kit (Thermo).NAD/NADH ratios and NADH levels were measured with the Amplite TM Flourimetric NAD/NADH Ratio Assay kit from (AAT Bioquest, #15263). The reaction was performed following the manufacturer's protocol.

4.11. Assessment of mitochondrial complex activities

Enzymatic activities for mitochondrial respiratory complexes were measured using previously described methods [65].

4.12. Blue native gel electrophoresis (BNGE)

The protein concentrations of isolated mitochondria were measured using PierceTM BCA Protein Assay kit (Thermo). Digitonin (DIG) at 4 g/g mitochondrial protein was used to solubilize the electron transfer chain complexes and 25 μg protein were applied and runon pre-cast NativePAGENovex 3%–12% Bis-Tris protein gels (Thermo Fisher Scientific) according to manufacturer's instructions [66]. After electrophoresis, the complexes were electroblotted onto PVDF membranes and sequentially probed with complex specific antibodies.

4.13. Recombinant adenoviral vectors expressing Pgc-1α

Adenovirus expressing PGC1α was generated using the AdEasy system. Briefly, the coding regions of mouse PGC1α were PCR amplified and subcloned into pAdTrack-CMV, resulting in pAdTrack-PGC1α. These shuttle vectors were used to generate recombinant adenoviruses (Ad-3 × Flag-PGC1α) as described previously [67].

4.14. shRNA

Plasmids encoding shRNAs were obtained from the MISSION *shRNA*

Library (Sigma Aldrich). The sequences of oligonucleotides were listed in Supplementary Table 1.

4.15. siRNA

Small interfering RNAs (siRNAs) (GenePharma) targeting mouse *Clpp*were transfected into differentiated myotubes at a final concentration of 175 nM using Lipofectamine 3000 according to the manufacturer's instructions. Cells were harvested 2 days post-transfection for analysis. The sequences of oligonucleotides were listed in Supplementary Table 1.

4.16. Statistical analysis

All experiments were carried out with multiple biological replicates. Assays involving cultured cells were performed with at least three independent replicates, and *in vivo* data were generated from at least three mice per genotype unless otherwise indicated. In some instances, representative images or results were shown. All values are the mean ± SEM. The statistics were performed with GraphPad Prism 8 software using an unpaired Student's *t*-test to compare two independent groups or pair for sequential measurements.

Author contributions

G.L. conceived and designed research; Y.Y.X. initiated the project and performed the mouse study and other experiments; Y.N.Z. and A.N. S. performed the proteolysis assay and other experiments; Y.M.P. performed the MEF experiments and provided assistance on other experiments; W.K.H. established the culture system; C.X., G.X.Z., X.S.H., Y.N. Z., F.F.Z. and F.W. performed experiments or provided assistance; Y.Y.X. Y.N.Z. and G.L. analyzed data; and Y.Y.X. and G.L. prepared and edited the manuscript.

Declaration of competing interest

The authors declare no conflict of interest in this report.

Acknowledgements

We wish to thank Drs. Ron DePinho (University of Texas M.D. Anderson Cancer Center) and Ying Cao (Nanjing University) for plasmids. G.L. wishes to thank Dr. Jianghuai Liu (Nanjing University) for critical reading of the manuscript. The work is supported by grants from National Key R&D Program of China (2019YFA0802803), National High-Tech R&D program of China (2014AA021606), Natural Science Foundation of China (31871433), the Fundamental Research Funds for the Central Universities (021414380524) and Nanjing University Double-First Class Initiative Fund to G.L. The work is also supported by grants from China Postdoctoral Science Foundation (2018M642212) and Jiangsu Planned Projects for Postdoctoral Research Funds to Y.Y.X.

Appendix A. Supplementary data

Supplementary data to this article can be found online at https://doi.org/10.1016/j.redox.2022.102447.

References

[1] N. Sun, R.J. Youle, T. Finkel, The mitochondrial basis of aging, Mol. Cell. 61 (2016) 654–666.
[2] H. Zhang, K.J. Menzies, J. Auwerx, The role of mitochondria in stem cell fate and aging, Development 145 (2018).
[3] V. Eisner, M. Picard, G. Hajnoczky, Mitochondrial dynamics in adaptive and maladaptive cellular stress responses, Nat. Cell Biol. 20 (2018) 755–765.
[4] J. Nunnari, A. Suomalainen, Mitochondria: in sickness and in health, Cell 148 (2012) 1145–1159.
[5] Y. Wang, S. Hekimi, Mitochondrial dysfunction and longevity in animals: untangling the knot, Science 350 (2015) 1204–1207.
[6] S. Ahola, T. Langer, T. MacVicar, Mitochondrial proteolysis and metabolic control, Cold Spring Harbor Perspect. Biol. 11 (2019).
[7] N. Pfanner, B. Warscheid, N. Wiedemann, Mitochondrial proteins: from biogenesis to functional networks, Nat. Rev. Mol. Cell Biol. 20 (2019) 267–284.
[8] M.J. Baker, T. Tatsuta, T. Langer, Quality control of mitochondrial proteostasis, Cold Spring Harbor Perspect. Biol. 3 (2011).
[9] P.M. Quiros, T. Langer, C. Lopez-Otin, New roles for mitochondrial proteases in health, ageing and disease, Nat. Rev. Mol. Cell Biol. 16 (2015) 345–359.
[10] Q. Zhao, J. Wang, I.V. Levichkin, S. Stasinopoulos, M.T. Ryan, N.J. Hoogenraad, A mitochondrial specific stress response in mammalian cells, EMBO J. 21 (2002) 4411–4419.
[11] A.M. Nargund, M.W. Pellegrino, C.J. Fiorese, B.M. Baker, C.M. Haynes, Mitochondrial import efficiency of ATFS-1 regulates mitochondrial UPR activation, Science 337 (2012) 587–590.
[12] T. Arnould, S. Michel, P. Renard, Mitochondria retrograde signaling and the UPR mt: where are we in mammals? Int. J. Mol. Sci. 16 (2015) 18224–18251.
[13] P.M. Quiros, M.A. Prado, N. Zamboni, D. D'Amico, R.W. Williams, D. Finley, S. P. Gygi, J. Auwerx, Multi-omics analysis identifies ATF4 as a key regulator of the mitochondrial stress response in mammals, J. Cell Biol. 216 (2017) 2027–2045.
[14] C. Cantó, K.J. Menzies, J. Auwerx, NAD(+) metabolism and the control of energy homeostasis: a balancing act between mitochondria and the nucleus, Cell Metabol. 22 (2015) 31–53.
[15] A.P. Gomes, N.L. Price, A.J. Ling, J.J. Moslehi, M.K. Montgomery, L. Rajman, J. P. White, J.S. Teodoro, C.D. Wrann, B.P. Hubbard, et al., Declining NAD(+) induces a pseudohypoxic state disrupting nuclear-mitochondrial communication during aging, Cell 155 (2013) 1624–1638.
[16] L. Mouchiroud, R.H. Houtkooper, N. Moullan, E. Katsyuba, D. Ryu, C. Canto, A. Mottis, Y.S. Jo, M. Viswanathan, K. Schoonjans, et al., The NAD(+)/Sirtuin pathway modulates longevity through activation of mitochondrial UPR and FOXO signaling, Cell 154 (2013) 430–441.
[17] S. Schiaffino, C. Reggiani, Fiber types in mammalian skeletal muscles, Physiol. Rev. 91 (2011) 1447–1531.
[18] P. Mishra, G. Varuzhanyan, A.H. Pham, D.C. Chan, Mitochondrial dynamics is a distinguishing feature of skeletal muscle fiber types and regulates organellar compartmentalization, Cell Metabol. 22 (2015) 1033–1044.
[19] A. Terskikh, A. Fradkov, G. Ermakova, A. Zaraisky, P. Tan, A.V. Kajava, X. Zhao, S. Lukyanov, M. Matz, S. Kim, et al., Fluorescent timer": protein that changes color with time, Science 290 (2000) 1585–1588.
[20] V.V. Verkhusha, D.M. Chudakov, N.G. Gurskaya, S. Lukyanov, K.A. Lukyanov, Common pathway for the red chromophore formation in fluorescent proteins and chromoproteins, Chem. Biol. 11 (2004) 845–854.
[21] A.W. Ferree, K. Trudeau, E. Zik, I.Y. Benador, G. Twig, R.A. Gottlieb, O.S. Shirihai, MitoTimer probe reveals the impact of autophagy, fusion, and motility on subcellular distribution of young and old mitochondrial protein and on relative mitochondrial protein age, Autophagy 9 (2013) 1887–1896.
[22] R.C. Laker, P. Xu, K.A. Ryall, A. Sujkowski, B.M. Kenwood, K.H. Chain, M. Zhang, M.A. Royal, K.L. Hoehn, M. Driscoll, et al., A novel MitoTimer reporter gene for mitochondrial content, structure, stress, and damage in vivo, J. Biol. Chem. 289 (2014) 12005–12015.
[23] K.M. Trudeau, R.A. Gottlieb, O.S. Shirihai, Measurement of mitochondrial turnover and life cycle using MitoTimer, Methods Enzymol. 547 (2014) 21–38.
[24] R.A. Gottlieb, A. Stotland, MitoTimer: a novel protein for monitoring mitochondrial turnover in the heart, J. Mol. Med. (Berl.) 93 (2015) 271–278.
[25] R.G. Whalen, D. Johnstone, P.S. Bryers, G.S. Butler-Browne, M.S. Ecob, E. Jaros, A developmentally regulated disappearance of slow myosin in fast-type muscles of the mouse, FEBS Lett. 177 (1984) 51–56.
[26] D.L. Allen, B.C. Harrison, A. Maass, M.L. Bell, W.C. Byrnes, L.A. Leinwand, Cardiac and skeletal muscle adaptations to voluntary wheel running in the mouse, J. Appl. Physiol. 90 (2001) 1900–1908. Bethesda, Md. : 1985.
[27] P. Mishra, V. Carelli, G. Manfredi, D.C. Chan, Proteolytic cleavage of Opa1 stimulates mitochondrial inner membrane fusion and couples fusion to oxidative phosphorylation, Cell Metabol. 19 (2014) 630–641.
[28] L.J. Reitzer, B.M. Wice, D. Kennell, Evidence that glutamine, not sugar, is the major energy source for cultured HeLa cells, J. Biol. Chem. 254 (1979) 2669–2676.
[29] K. Birsoy, R. Possemato, F.K. Lorbeer, E.C. Bayraktar, P. Thiru, B. Yucel, T. Wang, W.W. Chen, C.B. Clish, D.M. Sabatini, Metabolic determinants of cancer cell sensitivity to glucose limitation and biguanides, Nature 508 (2014) 108–112.
[30] S. Melser, E.H. Chatelain, J. Lavie, W. Mahfouf, C. Jose, E. Obre, S. Goorden, M. Priault, Y. Elgersma, H.R. Rezvani, et al., Rheb regulates mitophagy induced by mitochondrial energetic status, Cell Metabol. 17 (2013) 719–730.
[31] M. Mofarrahi, Y. Guo, J.A. Haspel, A.M. Choi, E.C. Davis, G. Gouspillou, R. T. Hepple, R. Godin, Y. Burelle, S.N. Hussain, Autophagic flux and oxidative capacity of skeletal muscles during acute starvation, Autophagy 9 (2013) 1604–1620.
[32] E.A. Moehle, K. Shen, A. Dillin, Mitochondrial proteostasis in the context of cellular and organismal health and aging, J. Biol. Chem. 294 (2019) 5396–5407.
[33] J. Ishizawa, S.F. Zarabi, R.E. Davis, O. Halgas, T. Nii, Y. Jitkova, R. Zhao, J. St-Germain, L.E. Heese, G. Egan, et al., Mitochondrial ClpP-mediated proteolysis induces selective cancer cell lethality, Cancer Cell 35 (2019) 721–737, e729.
[34] K.R. Pryde, J.W. Taanman, A.H. Schapira, A LON-ClpP proteolytic Axis degrades complex I to extinguish ROS production in depolarized mitochondria, Cell Rep. 17 (2016) 2522–2531.
[35] O. Hori, F. Ichinoda, T. Tamatani, A. Yamaguchi, N. Sato, K. Ozawa, Y. Kitao, M. Miyazaki, H.P. Harding, D. Ron, et al., Transmission of cell stress from

endoplasmic reticulum to mitochondria: enhanced expression of Lon protease, J. Cell Biol. 157 (2002) 1151–1160.
[36] M. Rep, J.M. van Dijl, K. Suda, G. Schatz, L.A. Grivell, C.K. Suzuki, Promotion of mitochondrial membrane complex assembly by a proteolytically inactive yeast Lon, Science 274 (1996) 103–106.
[37] A. Martin, T.A. Baker, R.T. Sauer, Protein unfolding by a AAA+ protease is dependent on ATP-hydrolysis rates and substrate energy landscapes, Nat. Struct. Mol. Biol. 15 (2008) 139–145.
[38] H. Shi, A.J. Rampello, S.E. Glynn, Engineered AAA+ proteases reveal principles of proteolysis at the mitochondrial inner membrane, Nat. Commun. 7 (2016), 13301.
[39] R. Rizzuto, D. De Stefani, A. Raffaello, C. Mammucari, Mitochondria as sensors and regulators of calcium signalling, Nat. Rev. Mol. Cell Biol. 13 (2012) 566–578.
[40] S. Austin, J. St-Pierre, PGC1α and mitochondrial metabolism–emerging concepts and relevance in ageing and neurodegenerative disorders, J. Cell Sci. 125 (2012) 4963–4971.
[41] Z. Arany, N. Lebrasseur, C. Morris, E. Smith, W. Yang, Y. Ma, S. Chin, B. M. Spiegelman, The transcriptional coactivator PGC-1beta drives the formation of oxidative type IIX fibers in skeletal muscle, Cell Metabol. 5 (2007) 35–46.
[42] S. Austin, E. Klimcakova, J. St-Pierre, Impact of PGC-1α on the topology and rate of superoxide production by the mitochondrial electron transport chain, Free Radical Biol. Med. 51 (2011) 2243–2248.
[43] J. Hoeks, Z. Arany, E. Phielix, E. Moonen-Kornips, M.K. Hesselink, P. Schrauwen, Enhanced lipid-but not carbohydrate-supported mitochondrial respiration in skeletal muscle of PGC-1α overexpressing mice, J. Cell. Physiol. 227 (2012) 1026–1033.
[44] J. St-Pierre, J. Lin, S. Krauss, P.T. Tarr, R. Yang, C.B. Newgard, B.M. Spiegelman, Bioenergetic analysis of peroxisome proliferator-activated receptor gamma coactivators 1alpha and 1beta (PGC-1alpha and PGC-1beta) in muscle cells, J. Biol. Chem. 278 (2003) 26597–26603.
[45] L. Guarente, Mitochondria–a nexus for aging, calorie restriction, and sirtuins? Cell 132 (2008) 171–176.
[46] N. Ivarsson, C.M. Mattsson, A.J. Cheng, J.D. Bruton, B. Ekblom, J.T. Lanner, H. Westerblad, SR Ca(2+) leak in skeletal muscle fibers acts as an intracellular signal to increase fatigue resistance, J. Gen. Physiol. 151 (2019) 567–577.
[47] C.S. Lee, D.K. Georgiou, A. Dagnino-Acosta, J. Xu, I.I. Ismailov, M. Knoblauch, T. O. Monroe, R. Ji, A.D. Hanna, A.D. Joshi, et al., Ligands for FKBP12 increase Ca2+ influx and protein synthesis to improve skeletal muscle function, J. Biol. Chem. 289 (2014) 25556–25570.
[48] R. Acín-Pérez, P. Fernández-Silva, M.L. Peleato, A. Pérez-Martos, J.A. Enriquez, Respiratory active mitochondrial supercomplexes, Mol. Cell. 32 (2008) 529–539.
[49] D. Moreno-Lastres, F. Fontanesi, I. García-Consuegra, M.A. Martín, J. Arenas, A. Barrientos, C. Ugalde, Mitochondrial complex I plays an essential role in human respirasome assembly, Cell Metabol. 15 (2012) 324–335.
[50] J. Durieux, S. Wolff, A. Dillin, The cell-non-autonomous nature of electron transport chain-mediated longevity, Cell 144 (2011) 79–91.
[51] R.C. Laker, J.C. Drake, R.J. Wilson, V.A. Lira, B.M. Lewellen, K.A. Ryall, C. C. Fisher, M. Zhang, J.J. Saucerman, L.J. Goodyear, et al., Ampk phosphorylation of Ulk1 is required for targeting of mitochondria to lysosomes in exercise-induced mitophagy, Nat. Commun. 8 (2017) 548.
[52] G. Hernandez, C. Thornton, A. Stotland, D. Lui, J. Sin, J. Ramil, N. Magee, A. Andres, G. Quarato, R.S. Carreira, et al., MitoTimer: a novel tool for monitoring mitochondrial turnover, Autophagy 9 (2013) 1852–1861.
[53] R. Anand, T. Wai, M.J. Baker, N. Kladt, A.C. Schauss, E. Rugarli, T. Langer, The i-AAA protease YME1L and OMA1 cleave OPA1 to balance mitochondrial fusion and fission, J. Cell Biol. 204 (2014) 919–929.
[54] P.P. Karunadharma, N. Basisty, Y.A. Chiao, D.F. Dai, R. Drake, N. Levy, W.J. Koh, M.J. Emond, S. Kruse, D. Marcinek, et al., Respiratory chain protein turnover rates in mice are highly heterogeneous but strikingly conserved across tissues, ages, and treatments, Faseb. J. 29 (2015) 3582–3592.
[55] S.E. Kruse, P.P. Karunadharma, N. Basisty, R. Johnson, R.P. Beyer, M.J. MacCoss, P.S. Rabinovitch, D.J. Marcinek, Age modifies respiratory complex I and protein homeostasis in a muscle type-specific manner, Aging Cell 15 (2016) 89–99.
[56] V.A. Lira, M. Okutsu, M. Zhang, N.P. Greene, R.C. Laker, D.S. Breen, K.L. Hoehn, Z. Yan, Autophagy is required for exercise training-induced skeletal muscle adaptation and improvement of physical performance, Faseb. J. 27 (2013) 4184–4193.
[57] E. Masiero, L. Agatea, C. Mammucari, B. Blaauw, E. Loro, M. Komatsu, D. Metzger, C. Reggiani, S. Schiaffino, M. Sandri, Autophagy is required to maintain muscle mass, Cell Metabol. 10 (2009) 507–515.
[58] S. Pickles, P. Vigie, R.J. Youle, Mitophagy and quality control mechanisms in mitochondrial maintenance, Curr. Biol. 28 (2018) R170–R185.
[59] L.C. Gomes, G. Di Benedetto, L. Scorrano, During autophagy mitochondria elongate, are spared from degradation and sustain cell viability, Nat. Cell Biol. 13 (2011) 589–598.
[60] A.S. Rambold, B. Kostelecky, N. Elia, J. Lippincott-Schwartz, Tubular network formation protects mitochondria from autophagosomal degradation during nutrient starvation, Proc. Natl. Acad. Sci. U. S. A. 108 (2011) 10190–10195.
[61] A.N. Crupi, J.S. Nunnelee, D.J. Taylor, A. Thomas, J.P. Vit, C.E. Riera, R. A. Gottlieb, H.S. Goodridge, Oxidative muscles have better mitochondrial homeostasis than glycolytic muscles throughout life and maintain mitochondrial function during aging, Aging 10 (2018) 3327–3352.
[62] G.D. Cartee, R.T. Hepple, M.M. Bamman, J.R. Zierath, Exercise promotes healthy aging of skeletal muscle, Cell Metabol. 23 (2016) 1034–1047.
[63] A. Safdar, J.M. Bourgeois, D.I. Ogborn, J.P. Little, B.P. Hettinga, M. Akhtar, J. E. Thompson, S. Melov, N.J. Mocellin, G.C. Kujoth, et al., Endurance exercise rescues progeroid aging and induces systemic mitochondrial rejuvenation in mtDNA mutator mice, Proc. Natl. Acad. Sci. U. S. A. 108 (2011) 4135–4140.
[64] K. Burkewitz, Y. Zhang, W.B. Mair, AMPK at the nexus of energetics and aging, Cell Metabol. 20 (2014) 10–25.
[65] M. Spinazzi, A. Casarin, V. Pertegato, L. Salviati, C. Angelini, Assessment of mitochondrial respiratory chain enzymatic activities on tissues and cultured cells, Nat. Protoc. 7 (2012) 1235–1246.
[66] P. Jha, X. Wang, J. Auwerx, Analysis of mitochondrial respiratory chain supercomplexes using blue native polyacrylamide gel electrophoresis (BN-PAGE), Curr. Protoc. Mol. Biol. 6 (2016) 1–14.
[67] J. Luo, Z.L. Deng, X. Luo, N. Tang, W.X. Song, J. Chen, K.A. Sharff, H.H. Luu, R. C. Haydon, K.W. Kinzler, et al., A protocol for rapid generation of recombinant adenoviruses using the AdEasy system, Nat. Protoc. 2 (2007) 1236–1247.